PERSEUS

POLICY-ORIENTED MARINE ENVIRONMENTAL RESEARCH IN THE SOUTHERN EUROPEAN SEAS

Comparative analysis of model simulations to assess SES resilience

Deliverable Nr. 4.9

Project Full title		Policy-oriented marine Environmental Research in the Southern EUropean Seas	
Project Acronym		PERSEUS	
Grant Agreement No.		287600	
Coordinator		Dr. E. Papathanassiou	
Project start date and duration		1st January 2012, 48 months	
Project website		www.perseus-net.eu	
Deliverable Nr.	4.9	**Deliverable Date**	December 2015
Work Package No		4	
Work Package Title		Developing integrated tools for environmental assessment.	
Responsible		Marco Zavatarelli (C0NISMa-UNIBO)	
Authors & Institutes Acronyms		M.Zavatarelli (CoNISMa-UNIBO), S. Libralato, C. Solidoro (OGS). C. Estournel (UPS-LA), K. Sagarakis (HCMR), I. Catalan (CSIC)	
Status:		**Final (F)**	•
		Draft (D)	
		Revised draft (RV)	
Dissemination level:		**Public (PU)**	•
		Restricted to other program participants (PP)	
		Restricted to a group specified by the consortium (RE)	
		Confidential, only for members of the consortium (CO)	

CONTENTS

EXECUTIVE SUMMARY / ABSTRACT

This deliverable reports the modelling results relative to the simulations carried out in “Scenario” modeto assess resilience in the dynamics of the lower and higher trophic levels dynamics of several sub-basin of the southern European Seas.

SCOPE

The deliverable aim is to provide an initial evaluation of the southern European Seas sensitivity at the regional scale, to changes in terrestrial inputs, affecting the lower trophic level dynamics, and to changes in the pressure exerted over the higher trophiic levels, including exploitation (fishery) pressure.

REGIONAL ASSESSMENT

Mediterranean Sea

Northern Adriatic Sea (CoNISMa-UNIBO)

Methodology

The used modelling system is based on the on-line coupling of the general circulation model NEMO (Nucleus for European Modelling of the Ocean; http://www.nemo-ocean.eu, version 3.4) with the lower trophic level biogeochemical Model BFM (Biogeochemical Flux Model, http://bfm-community.eu). The system is implemented in the Northern Adriatic Sea with a horizontal resolution of 800 m and 48 vertical z-levels. Surface forcing data were provided from ECHAM5 regional climate simulations (Scoccimarro et al., 2011). Initial conditions and open boundary data and, have been obtained from Mediterranean Sea circulation NEMO based simulations (Lovato et al., 2013), forced with the same atmospheric data used here. The land based river runoff and nutrient load data adopted considers 16 major Adriatic Rivers whose data were obtained from the PERSEUS Deliverable D4.3 Open boundary and initial conditions for BFM state variables were taken from BFM-POM (Princeton Ocean Model-Biogeochemical flux Model) Adriatic Sea simulations. The full NEMO-BFM coupling simulations span the period 1996-2010; here we show the results for the period 1996-2009.

The assessment carried out has been based on the ecosystem properties defining the ecosystem health: Vigor, Organisation, Resilience (Costanza and Mageau, 1999). Here the main emphasis is put on the “resilience” attribute.

River Forcing

The Northern Adriatic Sea resilience ha been evaluated with respect to changes in the land based (riverborne), since runoff and nutrient load is particularly important in determining the variability of the Marine ecosystem. The assessment is based on 5 different scenarios of river runoff and nutrient input based on the PERSEUS deliverable D6.4. A basic definition of the different scenarios is given below in table 1.

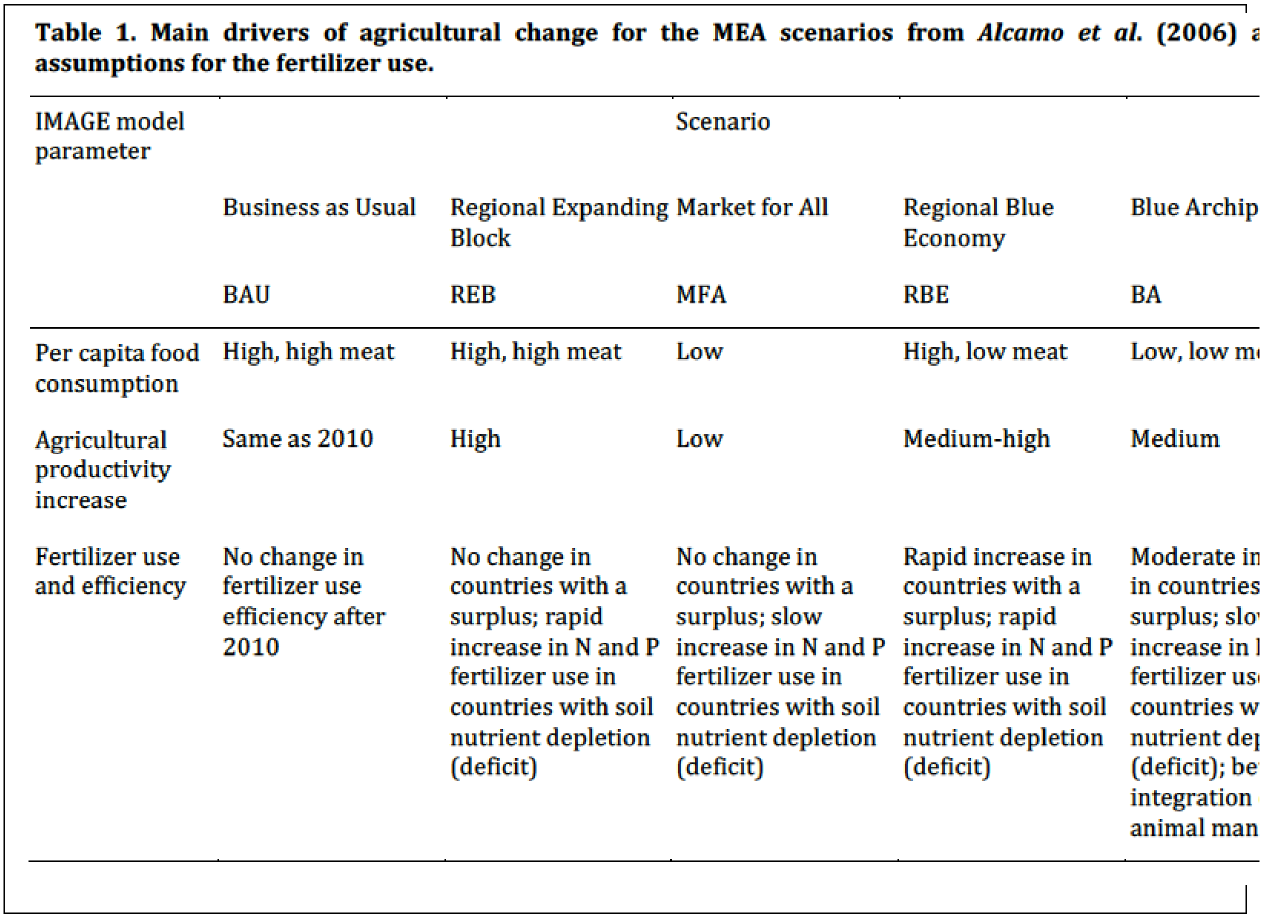

Table 1. Main drivers of agricultural change for the MEA scenarios from *Alcamo et al.* (2006) a assumptions for the fertilizer use.

IMAGE model parameter			Scenario		
	Business as Usual	Regional Expanding Block	Market for All	Regional Blue Economy	Blue Archip
	BAU	REB	MFA	RBE	BA
Per capita food consumption	High, high meat	High, high meat	Low	High, low meat	Low, low m
Agricultural productivity increase	Same as 2010	High	Low	Medium-high	Medium
Fertilizer use and efficiency	No change in fertilizer use efficiency after 2010	No change in countries with a surplus; rapid increase in N and P fertilizer use in countries with soil nutrient depletion (deficit)	No change in countries with a surplus; slow increase in N and P fertilizer use in countries with soil nutrient depletion (deficit)	Rapid increase in countries with a surplus; rapid increase in N and P fertilizer use in countries with soil nutrient depletion (deficit)	Moderate in in countries surplus; slo increase in fertilizer us countries w nutrient de (deficit); be integration animal man

The WP6 scenarios delineated in D6.4 were then translated into nutrient load data for the period 2000-2020 in WP4 and made available to WP4 partners trough deliverable D4.6. In order to provide the runoff and nutrient load data, a hydrological model was forced with the same atmospheric data (originating from a climate regional model) that were used here to force the Adriatic Sea model. The river runoff data and the correspondent nutrient load for the rivers pertinent to the northern Adriatic model domain were then used to force the Adriatic Sea coupled numerical model (Fig.1).

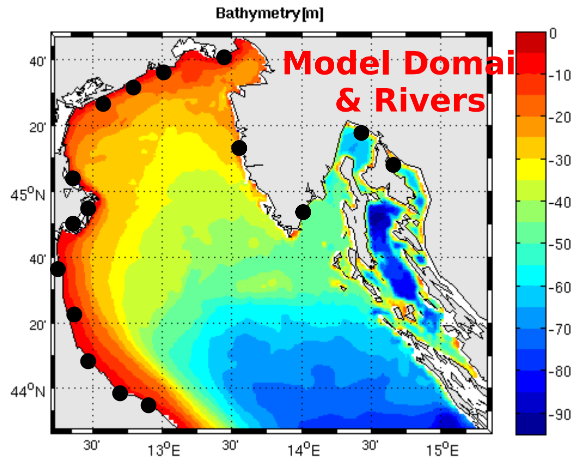

Fig.1: The northern Adriatic Sea models domain and bathymetry. Black dots indicate the location of the rivers discharging into the basin.

However, in order to assess the reliability of the projected simulations, a parallel hindcast simulation was carried out by forcing the model with the ERA-Interim atmospheric data and compared with the simulations results obtained from the use of the climate model data. Results of the comparison are shown in figure 2 with respect to the simulated sea surface temperature, chlorophyll-a and gross primary productivity.

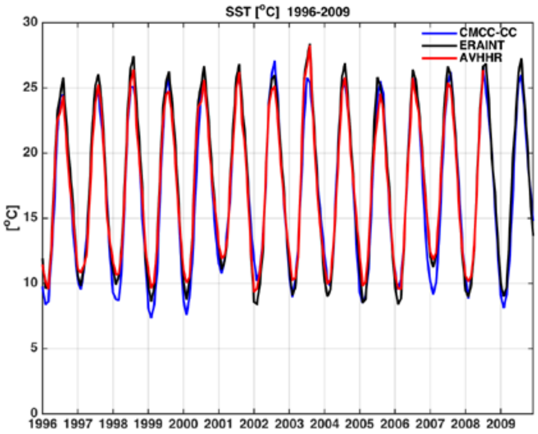

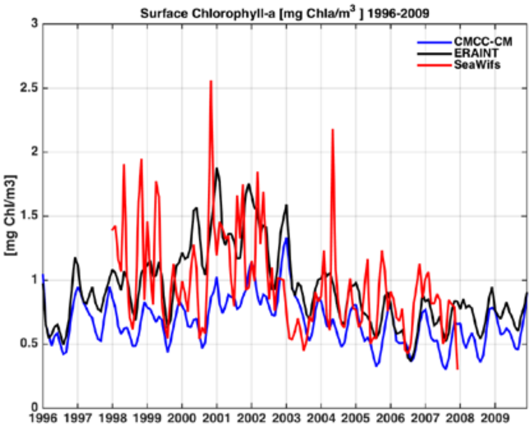

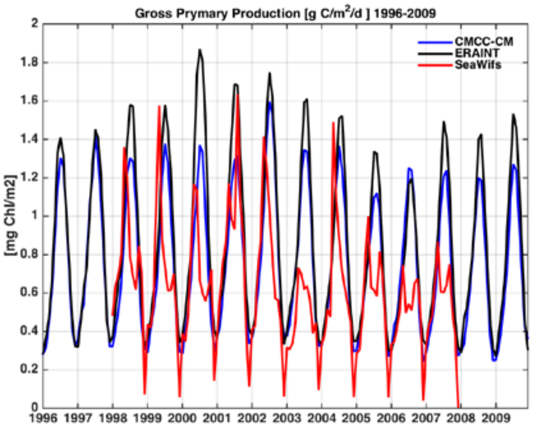

Fig.2: time series comparison of model results from climate model forcing (blue), ERA-interim forcing (black), AVHRR and seawifs satellite observations (red). Upper Panel: SST; Middle panel Chlorophyll-a; lower panel: Gross primary production.

Despite some differences an overall consistence between the two simulations results can be noted. This is further confirmed by the definition of the Taylor diagrams for the same properties that are reported in fig.3.

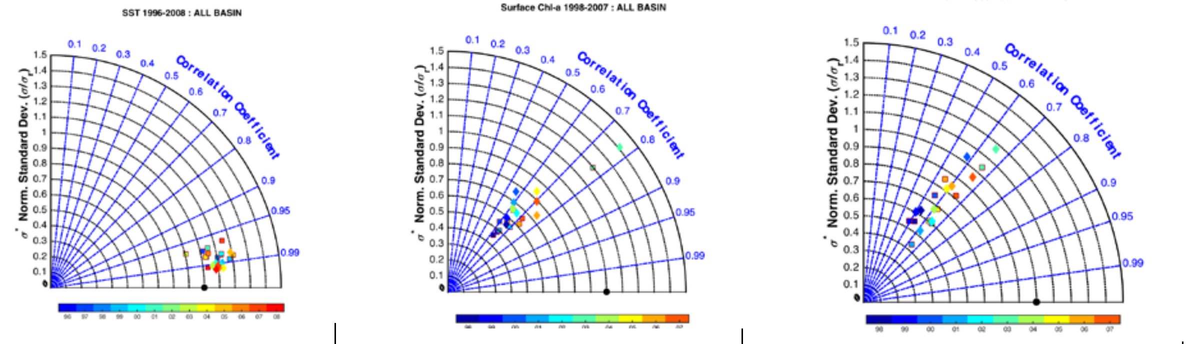

Fig.3: Taylor diagrams for the simulated SST (left), Chlorophyll (middle). Gross primary productivity (right). Squares: climate model forcing, Diamonds: ERA-interim forcing.

The figure indicates that the results from the two twin simulations have the same degree of correlations and the respective clusters tend to be superposed. The simulations projected ahead in time can be therefore considered reasonably reliable.

Each scenario simulation was run for the period 2000-2020 and the changes in term of Chlorophyll-a, gross primary production and secondary production from Micro and Mesozooplankton were assessed by computing the decadal averages (1999-2009 and 2010-2020) differences that are reported in figure 4.

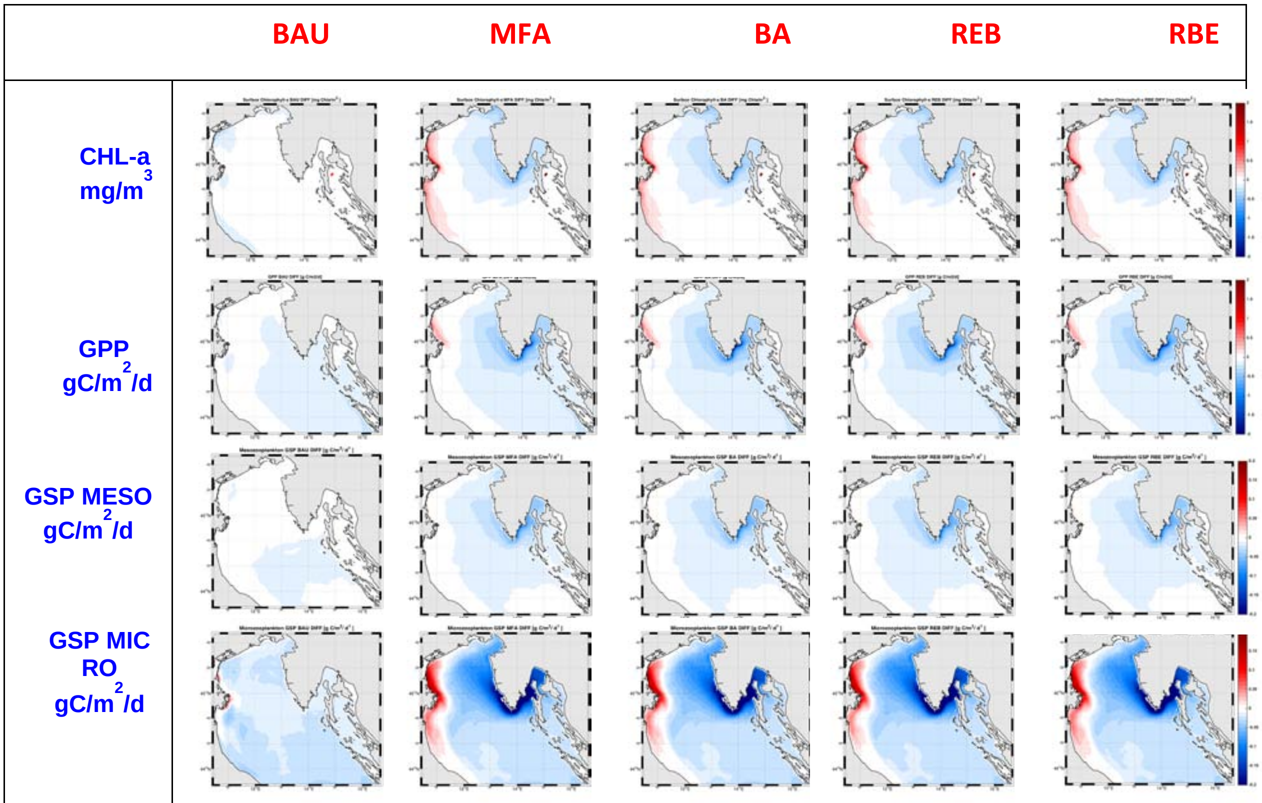

Fig. 4: simulations results for the 5 different nutrient load scenarios in term of decadal (1990-2009 and 2010-2020) averages differences.

It can be very easily noted that the differences between the hindcasted decade and the projections under the BAU (business as usual) scenarios are very minimal. This is in some sense expected since the BAU scenario assumes a continuation of the current trends. The differences between the hindcasted decade and the projected decade under the other four scenarios are very similar indicating that the difference scenarios in term of nutrient load are minimal and/or that the application time of a changed nutrient load is too short to produce a sensible difference in the dynamics of the lower trophic level ecosystem.

Adriatic Sea (OGS)

Further description of the Adriatic Sea Higher trophic level ecosystem is given also in Deliverables D4.8 and D4.12

The initial and boundary conditions in the numerical experiments

We adopted the MEDAR-MEDATLAS 2002 data set from a retrospective study performed during the MFSTEP project (Crise et al., 2003) with the purpose of finding the best initialization for the model simulation.

A Newtonian dumping term regulates the Atlantic buffer zone that is outside of the Strait of Gibraltar: the relaxed to climatological values derived from the MEDAR-MEDATLAS 2002 data set also.

Atmospheric deposition rates of inorganic nitrogen and phosphorus were set according to the synthesis proposed by Ribera d'Alcalà et al. (2003) and based on measurements of field data (Loye-Pilot et al., 1990; Guerzoni et al., 1999; Herut and Krom, 1996; Cornell et al., 1995; Bergametti et al.,1992). Atmospheric deposition rates of nitrate and phosphate were assumed to be constant during all the simulation, albeit with different values for the western (580 $KtNyr^{-1}$ and 16 $KtPyr^{-1}$) and eastern (558 $Kt\ N\ yr^{-1}$ and 21 $Kt\ P\ yr^{-1}$) sub-basins. The rates were calculated by averaging the ``low'' and ``high'' estimates reported by Ribera d'Alcalà et al. (2003).

The projections of terrestrial nutrient loads are based on future socio-economical scenarios of developments and the associated pressures on the Mediterranean Sea marine environment, in agreement with the PERSEUS deliverable D6.10 where BAU scenario and four alternative scenarios (REB,MFA, RBE,BA) for the period 2010-2020 are considered.

Table 1. Summary of the numerical experiment setup, external forcing functions and output data available for the project, the simulations has been carried out at the BlueGeneQ Fermi cluster at CINECA facilites.

OPATM-BFM	Value/Setup	Reference
Horizontal resolution	1/8°	Lazzari et al., 2012
Vertical resolution	3-600m (72 z levels)	Lazzari et al., 2012
Time step	1800 s	Lazzari et al., 2012
Horizontal Diffusion	Bilaplacian	Lazzari et al., 2012
Vertical turbulence scheme	As for MFS16-BFMc	
Biogeochemical model	BFM MedSea configuration	http://bfm-community.eu/
Forcing function	**Origin**	**Reference**
Atmospheric Fields	PO4 and NO3 input	Lazzari et al., 2012
Open boundary conditions	climatological seasonal profiles	Lazzari et al., 2012
River runoff	2000-2020 , PO4 NO3	PERSEUS D6.10
Initial conditions (BFM state variables)	MEDAR/MEDATLAS 2002 dataset	Lazzari et al., 2012
Physical forcing to compute transport	Water temperature, salinity, horizontal and vertical current velocities, vertical diffusion coefficient, MFS 2000-2020 1/16°, 72 levels, daily frequency (RCP8.5 scenario)	MFS16-BFMc (CMCC) model
Numerical Experiment	**Time window**	**Reference**
Spin up period	Starting from climatological conditions	Lazzari et al., 2012
Current Climate	2000-2009	CMIP5 observed Greenhouse gases
Scenario	2010-2020	
Outputs	**Description**	
Time frequency and type	monthly, NetCDF data	
3D state variables	3D maps of BFM biogeochemical variables	

Simulations Protocols

The simulations were carried out performing a spin-up of 5 years by repeating the year 2000 followed by a continuous simulation from 2000 to 2009 and terminating with the alternative scenarios for the decades from 2010 to 2020 as indicated in the Fig.2, the reference simulation uses the riverine BAU scenario produced by the D4.6 deliverable. The other 4 PERSEUS scenarios were carried out starting from the restart files produced for the 1st of January 2010.

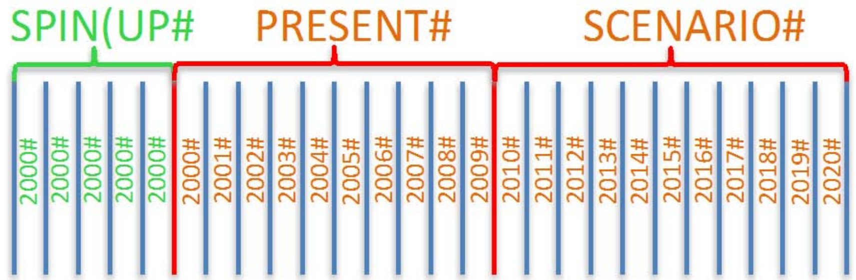

Figure 2 Simulation Scheme.

Simulation results: Comparison between the present simulation and the biogeochemical reanalysis.

We compared the results of PERSEUS-BaU simulation (CLI) with a reanalysis of the biogeochemical properties of the Mediterranean Sea (REA), performed in the myOcean/Copernicus/OPEC EU projects. In the numerical climate terminologies, a "reanalysis" is the results of a model simulation constrained by the available experimental observations through numerical techniques known as "data assimilation". In practice, a model is not let free to evolve in time according to its internal formulation and boundary conditions, but its evolution is corrected on the base of its agreement with available experimental information. In this way it is possible to integrate all the knowledge used to construct the numerical model (the theory) with all the experimental phenomenological information available (the practice), in order to produce the best estimate of the system's state and evolution. The reanalysis data can be seen also as interpolated data where the interpolation tool is the theoretical knowledge.

Clearly, it is possible to perform reanalysis only for the past, whereas no experimental data are available to constrain the model output. for the future state. The switch on-off of the data-assimilation for the past-future part of the simulation could potentially introduce an artificial bias by itself. Therefore for consistency reasons, climate simulations are wholly performed without data assimilation even if the initial part could be corrected with data. Nevertheless reanalysis can be used to test the level of realism of the climate simulation, and to asses the bias.

In fact, contrasting a climatic simulation for the contemporary conditions (2000-2009) versus a reanalysis reproducing the same period quantifies the climate model's skill in simulating the present. The extrapolation of this information for the future gives us an idea of the model's skill and realism in the scenario simulation (2010-2020). Still, a discrepancy between the CLI and the REA (the so called bias) does not imply that the estimates of the differences between scenario and present condition (the so called anomalies) provided by CLI are unrealistic. Insofar the discrepancy can be considered systematic, therefore affecting both contemporary and future simulations, the anomalies are realistic, and the future projection can be corrected by removing the bias. This procedure, named "bias correction procedure", is commonly adopted in climatic studies.

In the present Deliverable the REA is a biogeochemical simulation forced by the reanalysis of physical properties produced by the MFS16 ocean general circulation model (Adani et al., 2011). On top of this a variational data assimilation scheme (Teruzzi et al., 2014) is used to correct the dynamics of the biogeochemical properties by assimilating chlorophyll satellite data. In the framework of FP7 projects OPEC and MyOcean the REA results were corroborated using available data for cruises for the period 1998-2011. The comparison between CLI and REA are presented using four statistical indicators: the normalized bias (BIAS*), the correlation coefficients Rt, Rs (temporal and spatial), and the ratio between the standard deviations, Jolliff et al. (2009).

The BIAS* is expressed as:

$$BIAS^{*} = \frac{\overline{cli} - \overline{rea}}{\sigma_{rea}},$$

that corresponds to the difference of the average values of the contemporary condition simulation (*cli*) and of the reanalysis (*rea*), normalized over the standard deviation of the reference (σ_{rea}). The Rt is the correlation coefficient, basing on the seasonal evolution of the variables (inter annual variability is filtered out). $\sigma_{cli} / \sigma_{rea}$ is the ratio between the standard deviation of the climatic and reanalysis simulations.

For four selected variables and rates: phosphates, nitrates, chlorophyll and net primary production we statistically compared the representative seasonal cycle of CLI and REA for the 2000-2009 period, Tab.2. A fourth indicator Rs is considered in order to test if CLI and REA give consistent spatial patterns within each sub-basin considered. The sub-basins were defined to be relatively spatially homogenous regions, but still, there may be internal spatial variability in each sub-basin. Therefore the coherence in terms of spatial patterns is quantified by the Rs correlation indicator, calculated on the yearly averaged model output over a space grid and compared between CLI and REA. The mesh considered here is a 0.25 degree grid for the sub-basins and a 1 degree mesh for the whole Mediterranean basin (med).

The green(red) colors indicate whether(or not) the model skill is better than specific thresholds, that are: BIAS*< 1, Rt >0.7 (p=0.01), $0.5 < \sigma_{cli} / \sigma_{rea} < 2$ and Rs >0.04 (p=0.05).

A fifth indicator classifies and summarizes the model skill for each area: green (all indicators are green), yellow (three green indicators), pink (two green indicators), orange (one green indicator), red (no green indicator).

As it can be seen CLI well reproduces REA seasonal cycle both at the basin scale (med) and at the sub-basin scale, with lower accuracy for some sub-basins (marginal seas) and some variables. Phosphate presents an overall tendency to overestimate the values produced by the reanalysis (positive BIAS) on the contrary the indicators related to variability (temporal and spatial) are in good agreement for all the areas. Analogously, there is a general tendency of nitrates to overestimates as shown by the positive bias, and this signal is stronger in the case of nitrates than phosphates. In fact in the reanalysis we did an a-posteriori correction of nitrogen loads in the marginal seas (Adriatic and Aegean). In the present CLI simulations (PERSEUS) to preserve internal consistency in rivers nutrient loads we kept all the river data unchanged. Chlorophyll and in particular net primary productivity show a discrepancy in the temporal correlation Rt .essentially due to a systematic anticipation by the climate model of the maximum of productivity of two months. The within sub-basin spatial correlation always is very significant ($p<0.05$), with the exception of the chlorophyll for the ads sub-basin.

In conclusion, the overall agreement between CLI and REA can be considered good.

PO4

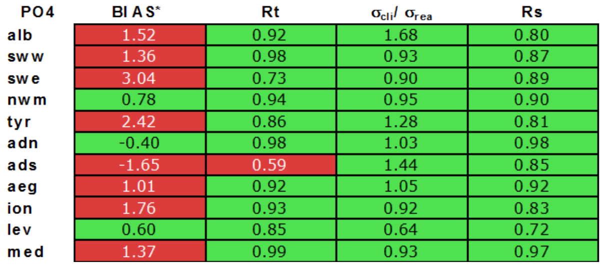

PO4	BIAS*	Rt	$\sigma_{cli}/\sigma_{rea}$	Rs
alb	1.52	0.92	1.68	0.80
sww	1.36	0.98	0.93	0.87
swe	3.04	0.73	0.90	0.89
nwm	0.78	0.94	0.95	0.90
tyr	2.42	0.86	1.28	0.81
adn	-0.40	0.98	1.03	0.98
ads	-1.65	0.59	1.44	0.85
aeg	1.01	0.92	1.05	0.92
ion	1.76	0.93	0.92	0.83
lev	0.60	0.85	0.64	0.72
med	1.37	0.99	0.93	0.97

NO3

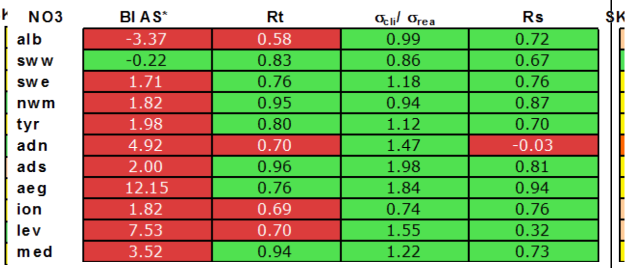

NO3	BIAS*	Rt	$\sigma_{cli}/\sigma_{rea}$	Rs
alb	-3.37	0.58	0.99	0.72
sww	-0.22	0.83	0.86	0.67
swe	1.71	0.76	1.18	0.76
nwm	1.82	0.95	0.94	0.87
tyr	1.98	0.80	1.12	0.70
adn	4.92	0.70	1.47	-0.03
ads	2.00	0.96	1.98	0.81
aeg	12.15	0.76	1.84	0.94
ion	1.82	0.69	0.74	0.76
lev	7.53	0.70	1.55	0.32
med	3.52	0.94	1.22	0.73

CHL

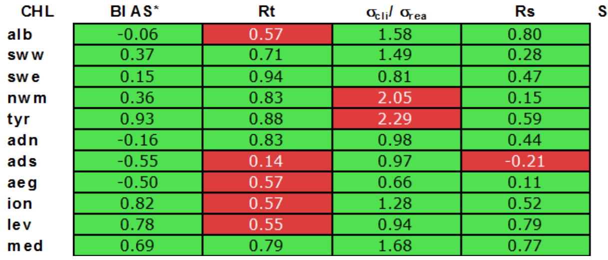

CHL	BIAS*	Rt	$\sigma_{cli}/\sigma_{rea}$	Rs
alb	-0.06	0.57	1.58	0.80
sww	0.37	0.71	1.49	0.28
swe	0.15	0.94	0.81	0.47
nwm	0.36	0.83	2.05	0.15
tyr	0.93	0.88	2.29	0.59
adn	-0.16	0.83	0.98	0.44
ads	-0.55	0.14	0.97	-0.21
aeg	-0.50	0.57	0.66	0.11
ion	0.82	0.57	1.28	0.52
lev	0.78	0.55	0.94	0.79
med	0.69	0.79	1.68	0.77

NPP

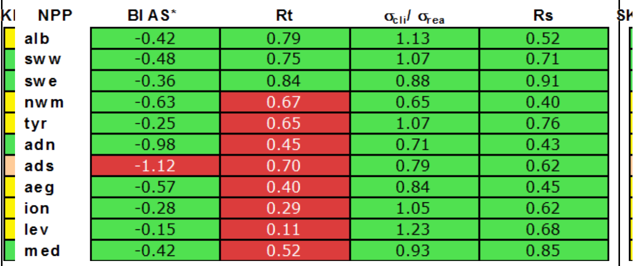

NPP	BIAS*	Rt	$\sigma_{cli}/\sigma_{rea}$	Rs
alb	-0.42	0.79	1.13	0.52
sww	-0.48	0.75	1.07	0.71
swe	-0.36	0.84	0.88	0.91
nwm	-0.63	0.67	0.65	0.40
tyr	-0.25	0.65	1.07	0.76
adn	-0.98	0.45	0.71	0.43
ads	-1.12	0.70	0.79	0.62
aeg	-0.57	0.40	0.84	0.45
ion	-0.28	0.29	1.05	0.62
lev	-0.15	0.11	1.23	0.68
med	-0.42	0.52	0.93	0.85

Table 2. Summary statistical indicators comparing the average seasonal cycles (BIAS*, Rt and $\sigma_{cli}/\sigma_{rea}$ columns) and average spatial distribution (Rs column) of the CLI and REA simulations. Nutrients are vertically integrated in layer 0-50 m whilst chlorophyll and net primary production are integrated in the layer 0-200 m. Green background color is assigned if $|\text{BIAS*}| < 1$, $Rt > 0.7$, $0.5<\sigma_{cli}/\sigma_{rea}<2$ and $Rs > 0.04$. The thresholds are assigned according to a T-test of $p=0.01$ for temporal trend and $p=0.05$ for spatial trend. In the fifth column of each table the color indicates a summary of the model skill for the specific area: green (four green indicators), yellow (three green indicators), pink (two green indicators), orange (one green indicator) and red (no green indicator). The spatial domain of each region is illustrated in Fig. 1.

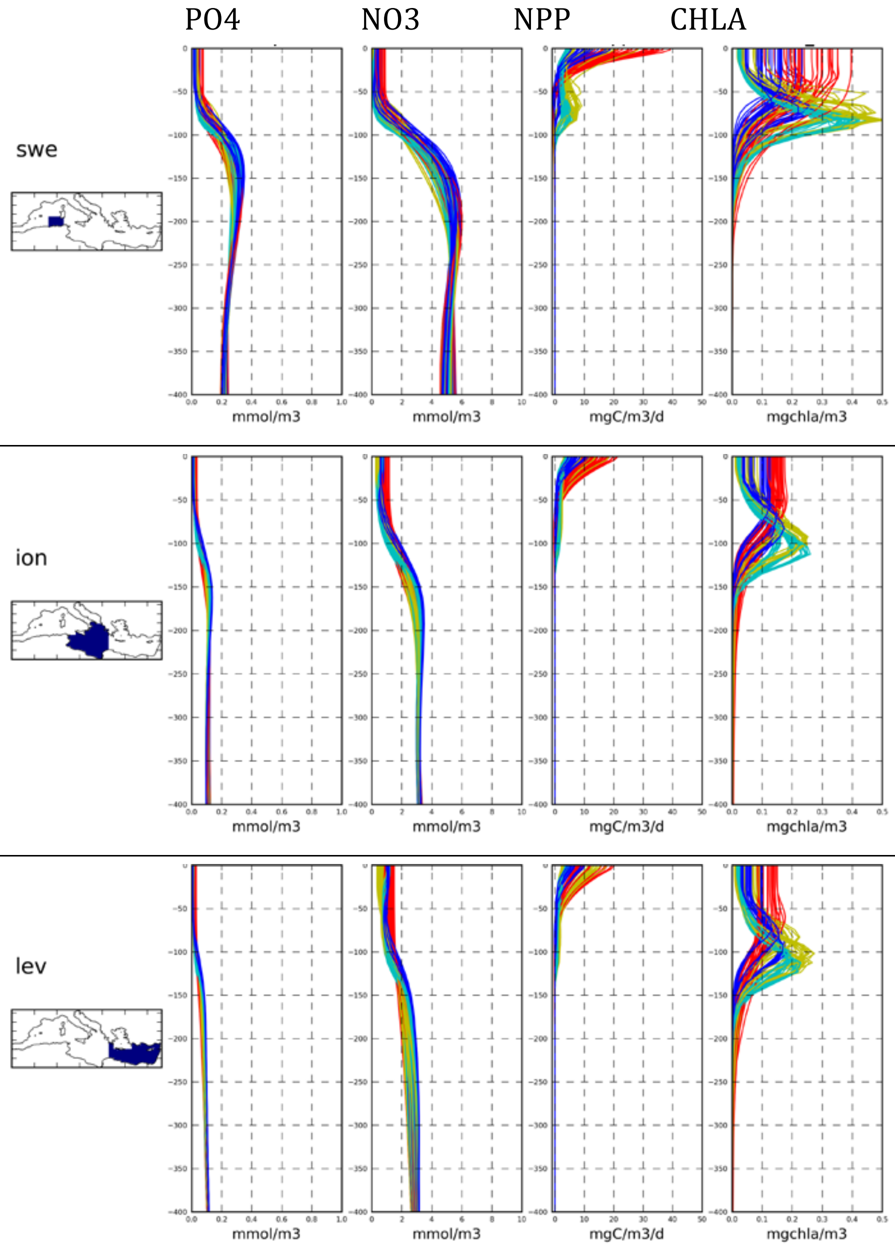

Figure 3. Nutrient profiles over selected sub-basins for the present period, each profile is a monthly mean, the color indicates the season (winter JFM-red, spring AMJ-yellow, summer JAS-cyan, fall OND-blue).

Simulation results: Comparison between present and future

Physical parameters derivations is discussed in full details in Lovato et al. 2013. The surface temperature anomaly (future - present) is positive in all areas and it is between 0.4 and 0.8 degrees Celsius. Surface salinity anomaly present both decrease and increase areas, the variability is in the range of +/- 0.5 PSU with higher increase in the Adriatic Sea and along the north eastern Ionian (images not shown, for further details see Lovato et al., 2013).

Moving to the biogeochemical properties the most important signals of spatial variability correspond to the vertical phosphate and nitrate gradients along the vertical dimension. This is due to the action of biological processes occurring in the euphotic zone and producing the typical vertical profile linked with the surface nutrients consumption. In Fig. 3 we reported the vertical profiles of chlorophyll, nitrate and phosphate averaged over representative sub-regions (as selected examples of Mediterranean area trophic gradient) like a western sub-basin (SWE), a central sub-basin (INO) and an eastern sub-basin (LEV). .

In the layers below 1000 m the nutrient concentrations are stable at seasonal and decadal temporal scales. The winter mixing phase is evident (red profiles) in all the sub-basins with higher chlorophyll values according to the west east trophic gradients.

During the summer period the deep chlorophyll maximum (DCM - cyan profiles) appears at different depths: from the 70 m depth in the SWE sub-basin 100 m for the ION reaching 120 m in the Levantine sub-basin. Nitrate concentration does not present a clear west east gradient in the upper layer but the west east gradient appears in the sub-surface layers, below 100 m depth. On the contrary in the case of phosphates the west east gradient is present also at surface. For phosphates and nitrates both, the nutricline depth during the summer period is controlled by the plankton dynamics and therefore it correlates with the chlorophyll profile, and it becomes deeper moving eastward. According to the vertical distribution of nutrient and chlorophyll, Fig.3, we considered surface integrated nutrient on the layer 0-50 meters to have a statistically homogenous vertical averaging or integrating .

In the following, a comparison among present and scenario (BaU) estimates of major biogeochemical properties is illustrated by means of several spatial distribution maps.

A summary of the results is presented by bi-dimensional maps of mean or integrated concentrations for the present (period 2000-2009) compared to future projections (2010-2020), first. Then spatial distributions of absolute anomalies (future-present) are shown for the four seasons. Finally, the 20 years time series of the spatially aggregated data are shown on three selected sub-basins.

Nutrients distributions: phosphate and nitrate

Results of the present condition averaged for the years 2000-2010 (Fig. 4 left panel) show that the horizontal patterns and gradients are essentially associated with the thermohaline circulation of the Mediterranean Sea and its anti-estuarine behavior: the upper thermohaline cell generates a net nutrient outflow from the Mediterranean Sea basin. Eastern areas are affected to an higher extent by this depletion effect, also due to the different inflow of terrestrial inputs. Therefore a progressive increase in oligotrophy moving eastward from Alboran Sea region toward the Levantine region is observed. The nutrient inputs from terrestrial and atmospheric origin are in general phosphorus depleted and in general, a phosphorus limitation sets up in the Mediterranean Sea marine system. The marginal seas (Adriatic and Aegean) show a peculiar dynamics because they are strongly affected by terrestrial inputs.

The present condition map of phosphates, Fig.4 left panel, shows that from the Alboran Sea, a signal, relatively rich in phosphate, propagates eastward detaching from the Algerian coast. Al the western basin presents higher values than the rest of the basin, with a reduction in the Tyrrhenian and a marked drop of concentration crossing the Sicily Strait. along the Algerian current reaching the Sicily Straits. The phosphate enrichment is present also in Gulf of Lions and in the southern Adriatic gyre, even if the mixing intensity due to the convective chimneys is not extremely pronounced . On the contrary the anti-cyclonic gyres, located in the southern Levantine area and more extensively a rim area characterizing all the Levantine region and southern Aegean Sea, exhibit the lowest nutrient concentrations.

The properties shown by the model simulation are coherent with the available in situ measurements accomplished in the last decades, reviewed by Siokou-Frangou et al. (2010), and from the synthesis on spatial and temporal averaged vertical profiles for the Mediterranean biogeochemical properties 1950-2000 (Manca et al.; 2004). This information present in the MEDAR-MEDATLAS dataset was in part used to derive the initial conditions of the model.

The Scenario surface phosphate distributions (2010-2020, Fig.4 right panel) are qualitatively similar to the present condition distributions (2000-2009, Fig.4 left panel).

The absolute anomaly (future – present), Fig.5, shows that during the winter season the higher positive anomaly is located around the Alboran Sea area, in correspondence of the North Western Mediterranean area and in the northeastern Ionian Sea. In most of the areas of the Mediterranean Sea the anomaly is positive, with only two negative spots in the deep mixing area of the Gulf of Lions and in the Tyrrhenian Sea. The anomaly map presents a patchy structure with the highest anomaly lower than 0.02 mmol P m^{-3}.

Apart from the North Aegean the signal of river load increase (e.g. North Western Med) is not evident and of second order with respect to open ocean dynamics.

The time series of the averaged phosphate for the Mediterranean Sea, for the NWM and for the LEV, show all a dominant signal related to the seasonal variability super-imposed to a relevant, inter-annual variability. In particular on Mediterranean scale an increasing trend is evident, discriminating the first from the second simulation decades. For the NWM the signal is less clear even if, as seen from the averaged map the tendency is of decreasing the phosphate inventory. The Levantine sub-basin shows an increasing trend with a stabilized regime in the 2010-2020 decade.

The surface nitrate present similar patterns as the case of the phosphate. Fig.7.

The scenario simulation (2010-2020) indicates a decrease of nitrate concentrations in the western basins whilst an increase is simulated for the eastern basins. Also the anomaly maps, Fig. 8, indicates similar patterns with respect to phosphate. The strong decrease of nitrogen accumulation in the 0-50 meter vertical average is not present if we consider the 0-200 averaged values. For the whole Mediterranean the nitrogen anomaly variability is mostly confined to values in the range [-1,1] mmol N m^{-3}.

The nitrate time series of the whole Mediterranean basin (Fig. 9, top panel) indicates that also in the case of nitrates the seasonal variability is the dominant temporal signal. The inter-annual variability is also important. The period 2000-2005 period shows a stable trend followed by a period of increase and then a stabilization.

The time series for the NWM sub-basin (Fig. 9, middle) shows also a marked seasonal cycle and a strong inter-annual. In the LEV sub-basin (Fig. 9, bottom) we observe an increase a stabilization during the last five years of the simulation. The comparison of nutrient distributions for the 4 alternative scenarios indicates second order effect if compared with the anomalies between present and future scenario, image not shown.

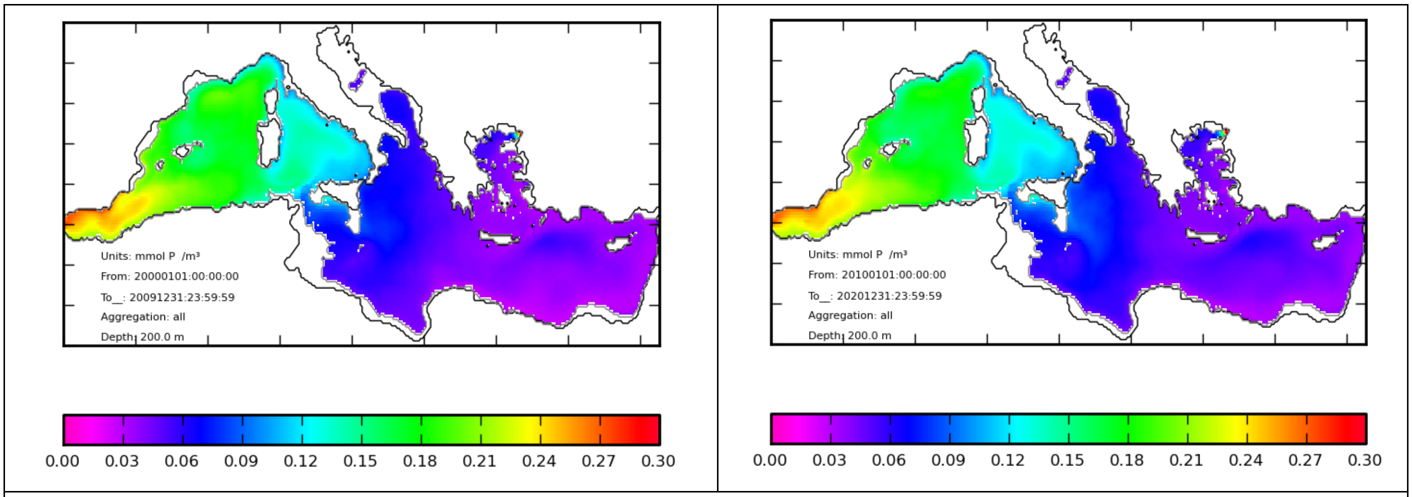

Figure 4. Mean phosphate concentration expressed in mmol P m^{-3} averaged over the upper 200 m depth, for the period 2000-2010 (left), and for the period 2010-2020 (right).

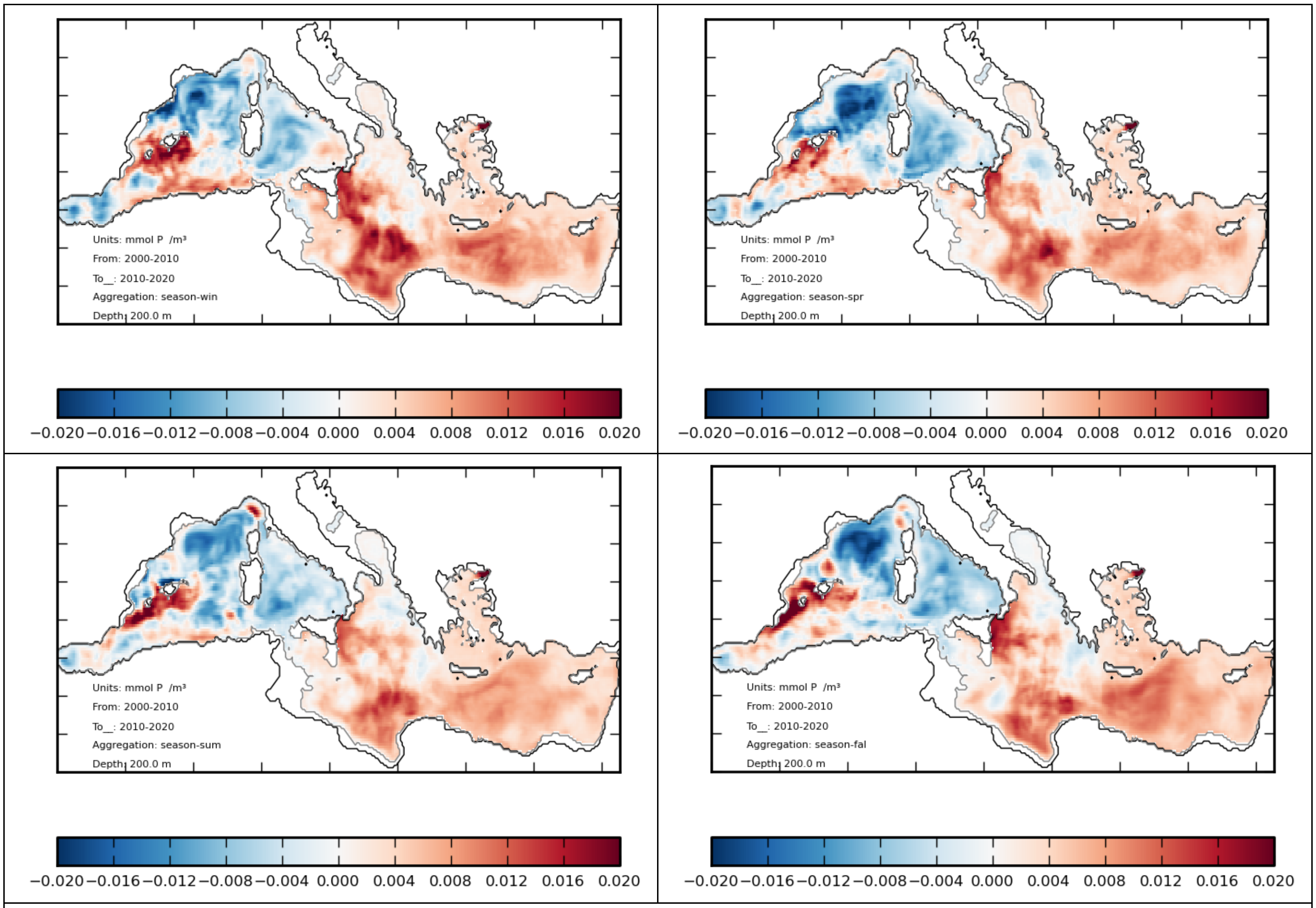

Figure 5. Phosphate concentration absolute anomalies expressed in mmol P m^{-3} (scenario(2010-2020) – present (2000-2010)) averaged over the upper 200 m depth. Anomalies are aggregated for the different seasons: Winter (Jan-Feb-Mar) top left, Spring (Apr-May-Jun) top right, Summer (Jul-Aug-Sep) bottom left, Autumn (Oct-Nov-Dec)

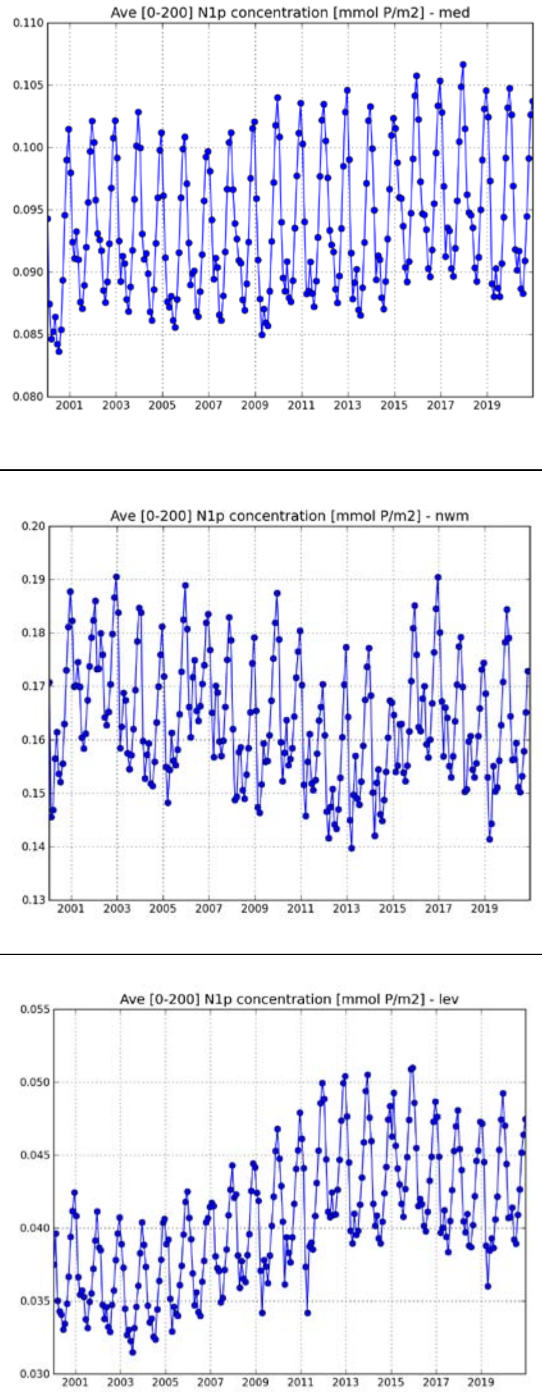

Figure 6. Time series of surface (0-200 m) average phosphates concentration of the scenario simulation from OPATM-BFM model for selected sub –regions

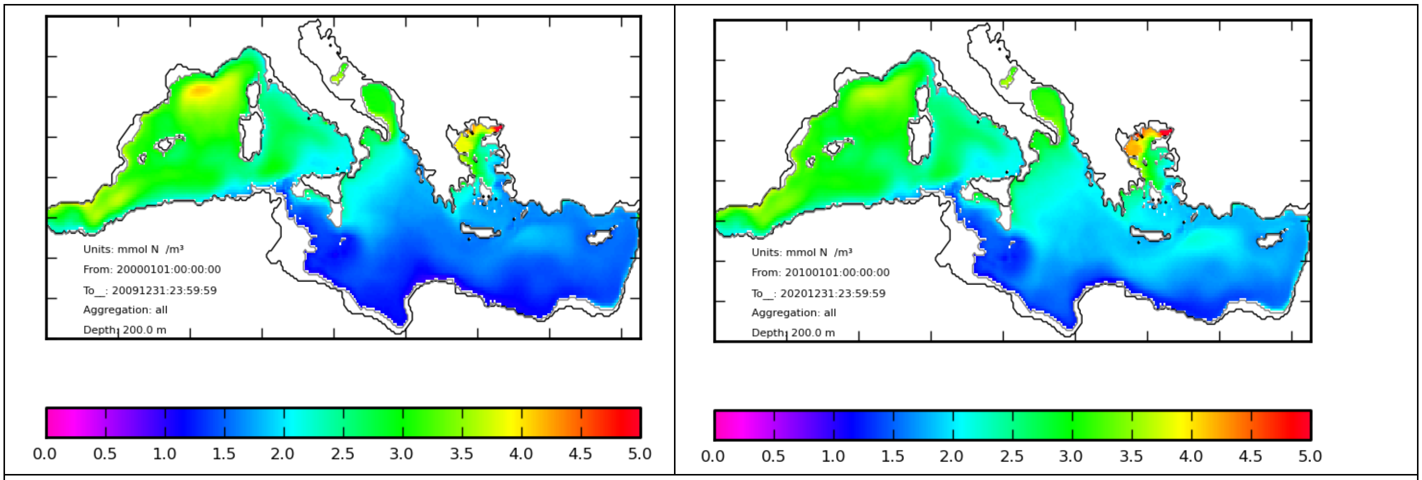

Figure 7. Nitrate concentration expressed in mmol N m^{-3} averaged over the upper 200 m depth, left for the period 2000-2010, right for the period 2010-2020.

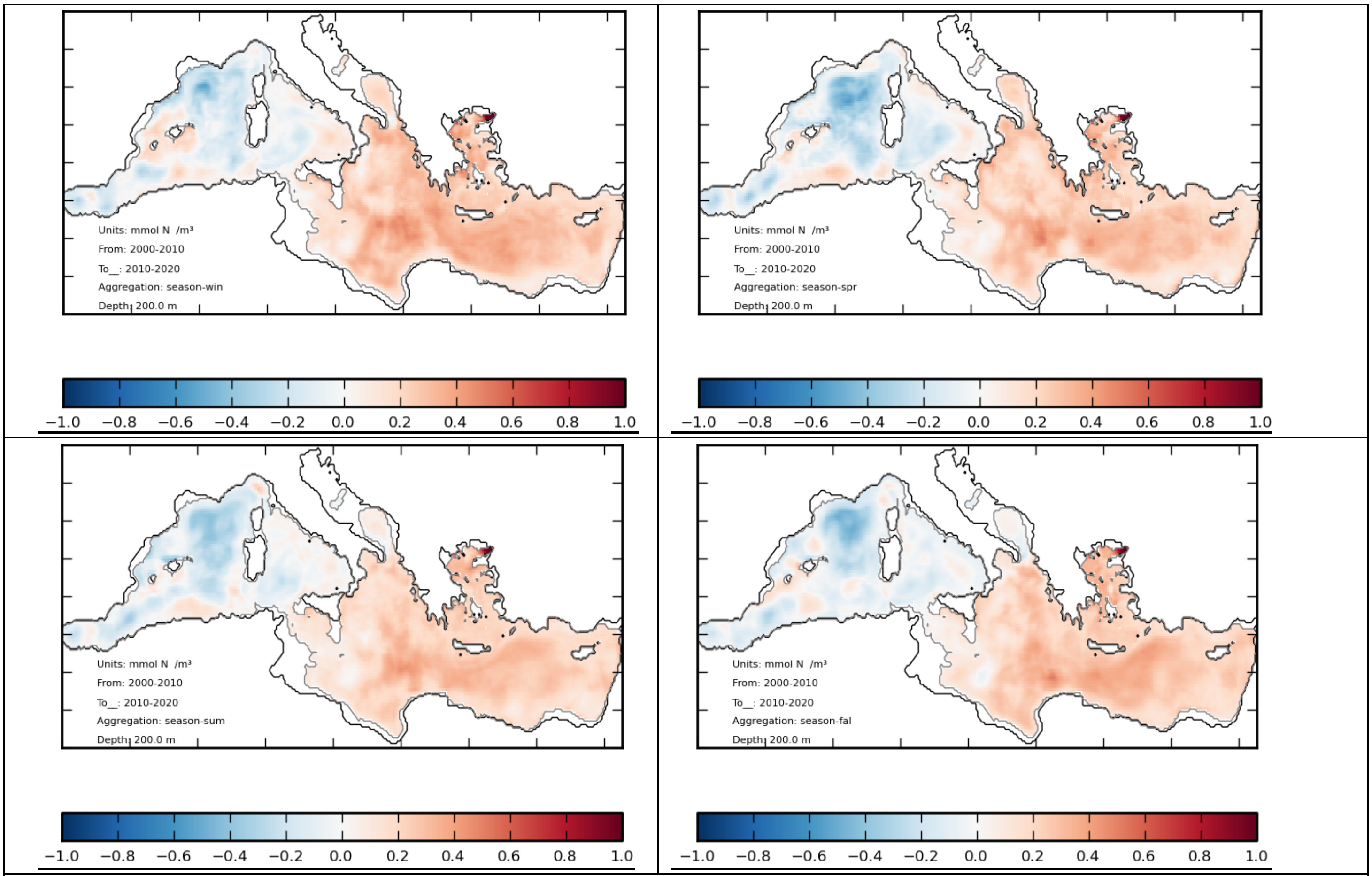

Figure 8. Nitrate concentration absolute anomalies expressed in mmol N m^{-3} (scenario(2010-2020) – present (2000-2010)) averaged over the upper 200 m depth. Anomalies are aggregated for the different seasons: Winter (Jan-Feb-Mar) top left, Spring (Apr-May-Jun) top right, Summer (Jul-Aug-Sep) bottom left, Autumn (Oct-Nov-Dec) bottom right

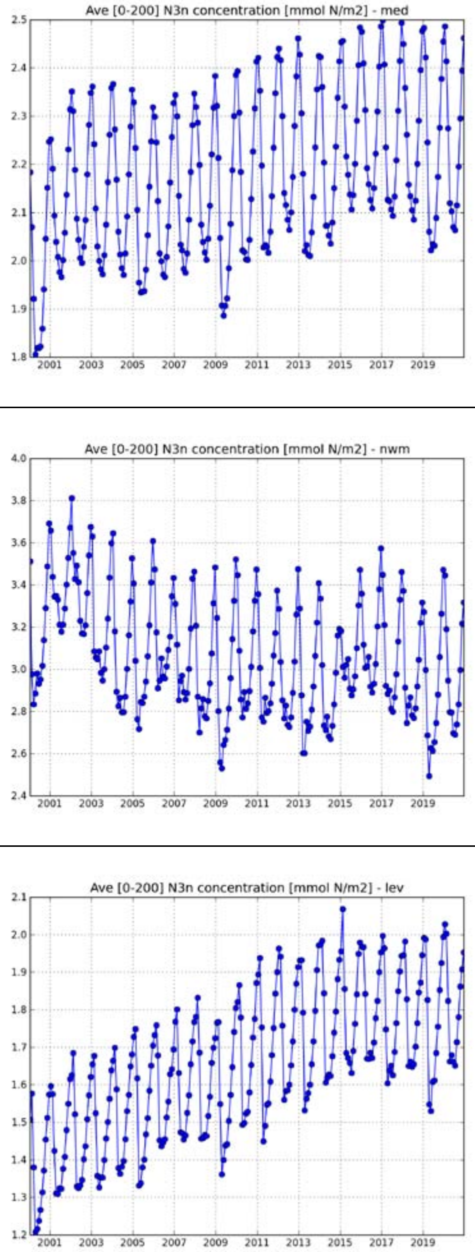

Figure 9. time series of surface (0-200 m) phosphates of the scenario simulation from OPATM-BFM model for selected sub–regions

Chlorophyll and primary production

Due to its specific nutrients regimes the Mediterranean Sea is classified as one of the most oligotrophic regions of the world (Azov, 1991). Satellites based chlorophyll elaborations show clearly a negative west-east trend in the surface chlorophyll concentrations (Bosc et al., 2004; Volpe et al., 2007; Barale et al., 2008; D'Ortenzio and Ribera d'Alcalà, 2009), this dominant basin scale signature is also congruent with the available, unfortunately sparse, in situ measurements (Turley et al., 2000). Model results reflect this general pattern, showing a congruent longitudinal pattern, Fig. 10.

In the present simulation the chlorophyll and NPP distributions are integrated along the upper 200m therefore the shallow areas (depth lower than 200 m) are masked out.

The anomaly maps, Fig. 11, show patchy areas of increment/decrease. The winter period presents the higher differences in the future scenario largely in the range [-4,+4] mg chl m^{-2} . There is no a clear anomaly pattern with the exception of an increase in north western area a decrease in correspondence of the south Adriatic gyre and an increase again in the Aegean. Some mild increase signal appear also in the winter panel in correspondence of the Rhodes gyre area and in general the Levantine area presents a positive anomaly.

Also in the case of chlorophyll the temporal variability presents a dominant seasonal cycle but also the inter-annual variability in the maximum of chlorophyll is relevant and both overcome the trends over decadal time scale, Fig. 12. Same arguments are valid for NWM and LEV sub basins.

The summer deep chlorophyll maximum (DCM), Fig. 16, also presents both a west east gradient and a north south one with shallower DCM in the area of the Alboran Sea (30 meters), and deeper DCM in the southern Levantine area shallower in the western area and deeper moving eastward: 30 meters in the Alboran Sea area and 120 meters in the Levantine area.

The scenario projection for 2010-2020 indicates that DCM will change more during the winter period when indeed the maximum of chlorophyll is very near the surface and during the stratification period the changeof the DCM is of the order of few meters. (Fig. 13).

Integrated Net primary productivity shows also a clear (NPP) pattern, Fig. 14, evidencing the longitudinal trophic gradient.The area of the Alboran Sea presents the higher productivity rates. Also in the area of the Sicily channel patchy structures of high productivity are present and are related to upwelling processes. The Aegean Sea and a rim area around the north and eastern part of the Mediterranean Sea presents a marked oligotrophic regime.

The scenario for the period 2010-2020 present similar anomalies as chlorophyll with patchy structures of positive negative anomalies more marked during the winter period.

The time series of NPP presents also a marked seasonal cycle, and a significant inter-annual variability of the maximum annual values, Fig. 15.

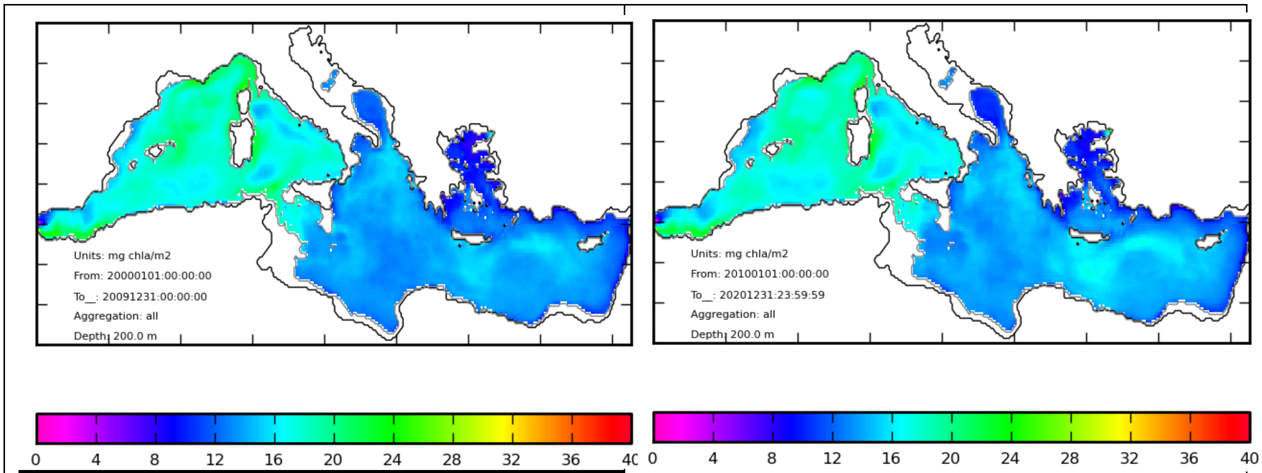

Figure 10 Vertically integrated total chlorophyll expressed in mg chl m^{-2} over the upper 200 m depth, for the period 2000-2010 (left panel) and for the period 2010-2020 (right panel).

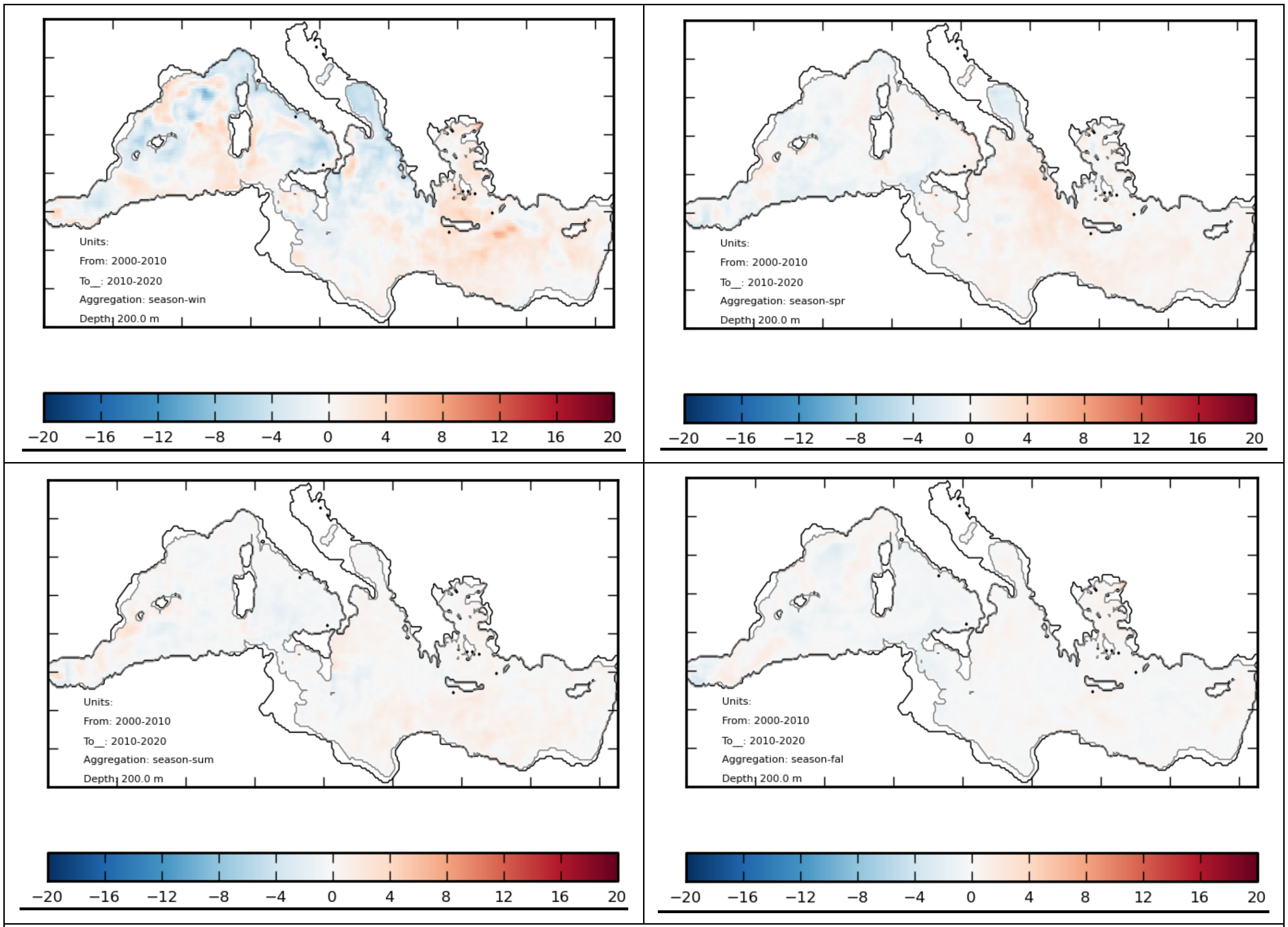

Figure 11. integrated chlorophyll absolute anomalies expressed in mgchla m^{-2} (scenario(2010-2020) – present (2000-2010)) averaged over the upper 200 m depth. Anomalies are aggregated for the different seasons: Winter (Jan-Feb-Mar) top left, Spring (Apr-May-Jun) top right, Summer (Jul-Aug-Sep) bottom left, Autumn (Oct-Nov-Dec) bottom right

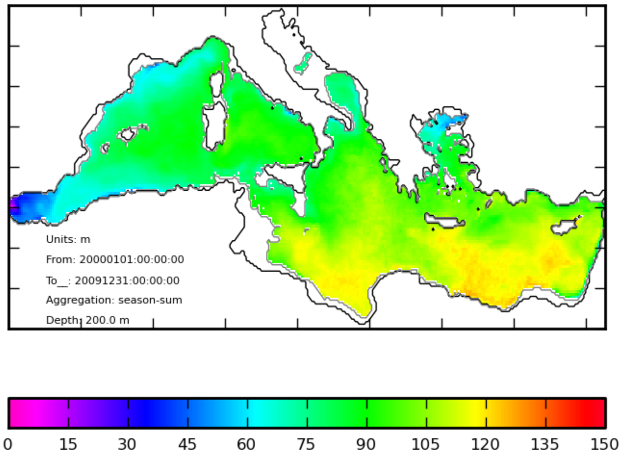

Figure 12 Deep chlorophyll maximum expressed m for the summer season (Jul-Aug-Sep), for the period 2000-2010 (left panel) and for the period 2010-2020 (right panel).

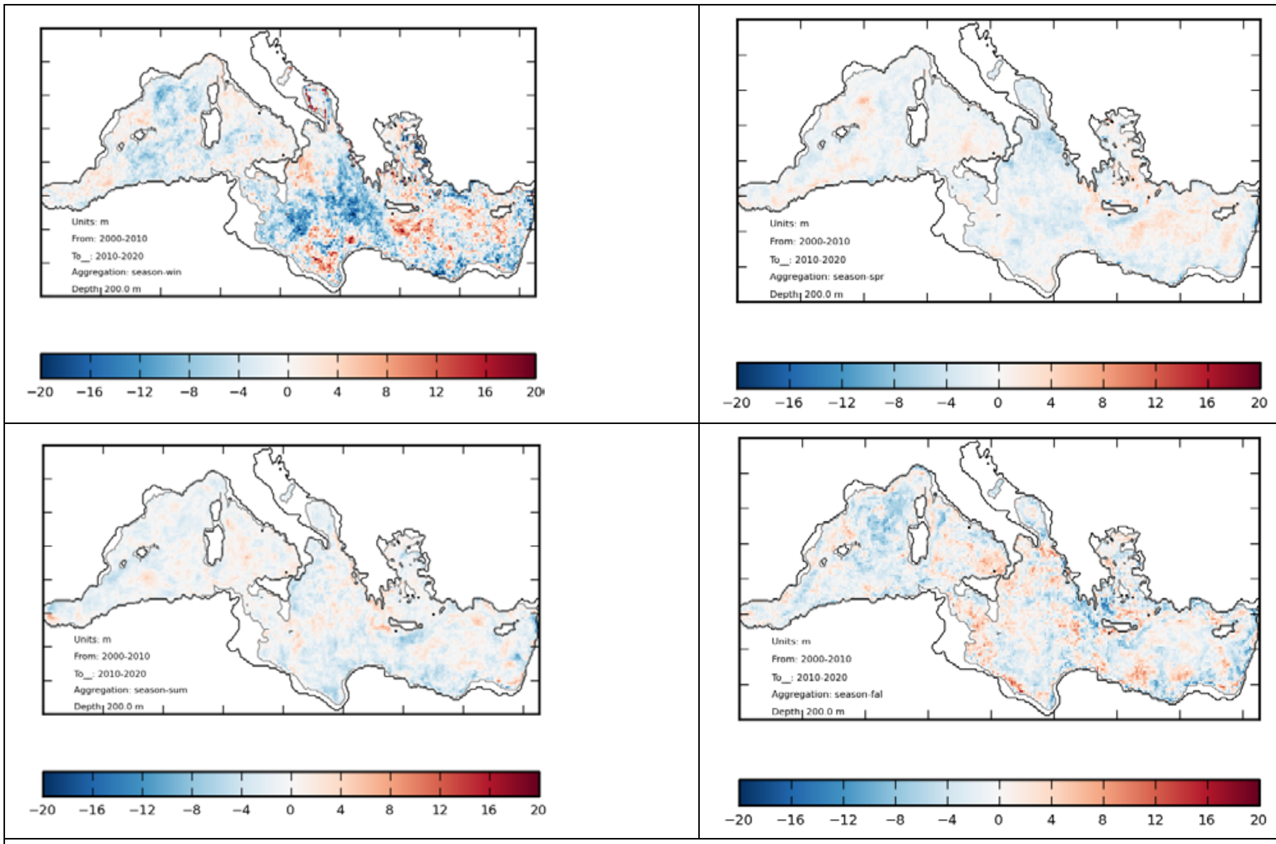

Figure 13. Deep chlorophyll maximum (DCM) absolute anomalies expressed in m (scenario(2010-2020) – present (2000-2010)). Positive values indicate a deepening of the DCM in the future, negative values indicate a DCM becoming shallower. Anomalies are aggregated for the different seasons: Winter (Jan-Feb-Mar) top left, Spring (Apr-May-Jun) top right, Summer (Jul-Aug-Sep) bottom left, Autumn (Oct-Nov-Dec) bottom right

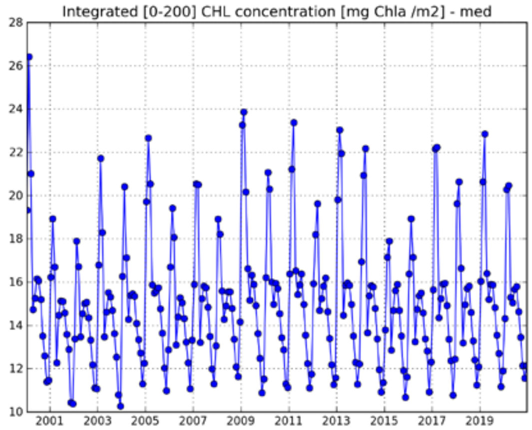

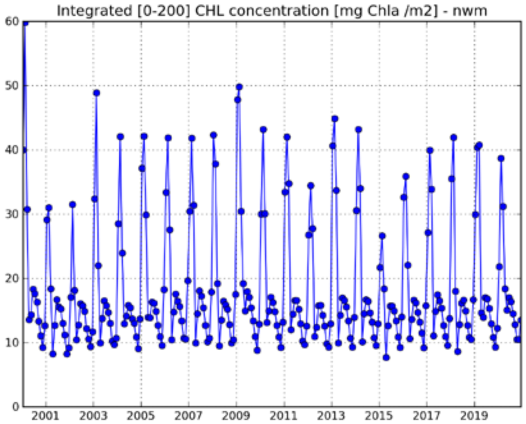

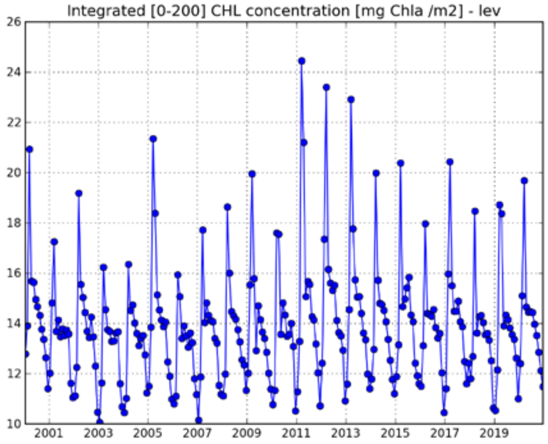

Figure 14. Time series of vertically integrated chlorophyll (0-200 m) expressed in mg chla m^{-2} of the scenario simulation from OPATM-BFM model averaged over the entire Mediterranean Sea basin, the western sub-basin and eastern sub –basin

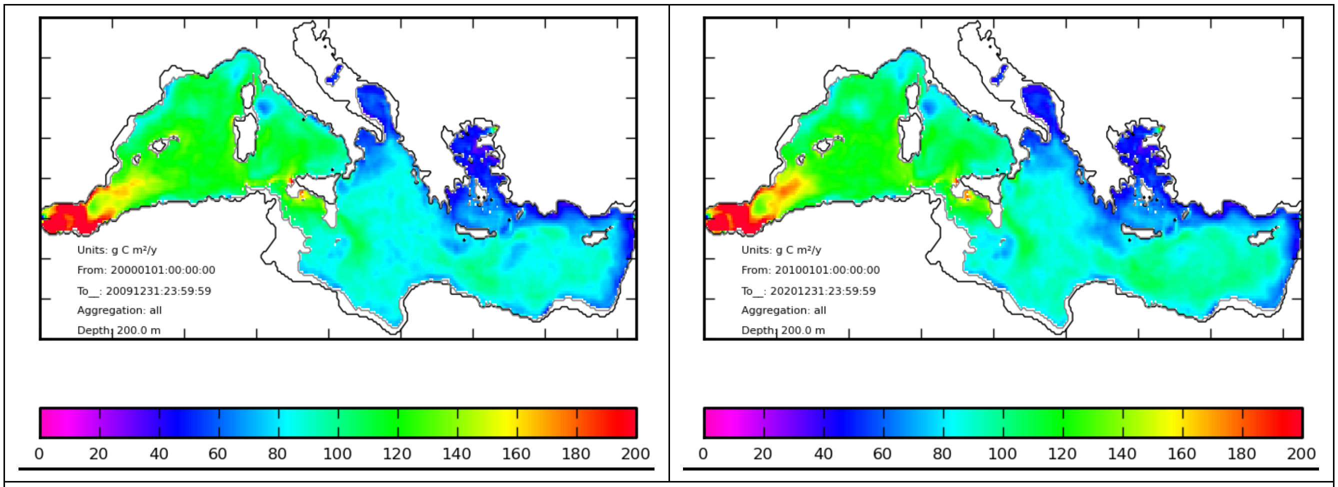

Figure 16 Integrated Net primary production over the upper 200 m depth expressed in gC m^{-2} y^{-1}, for the period 2000-2010 (left panel) and for the period 2010-2020 (right panel)

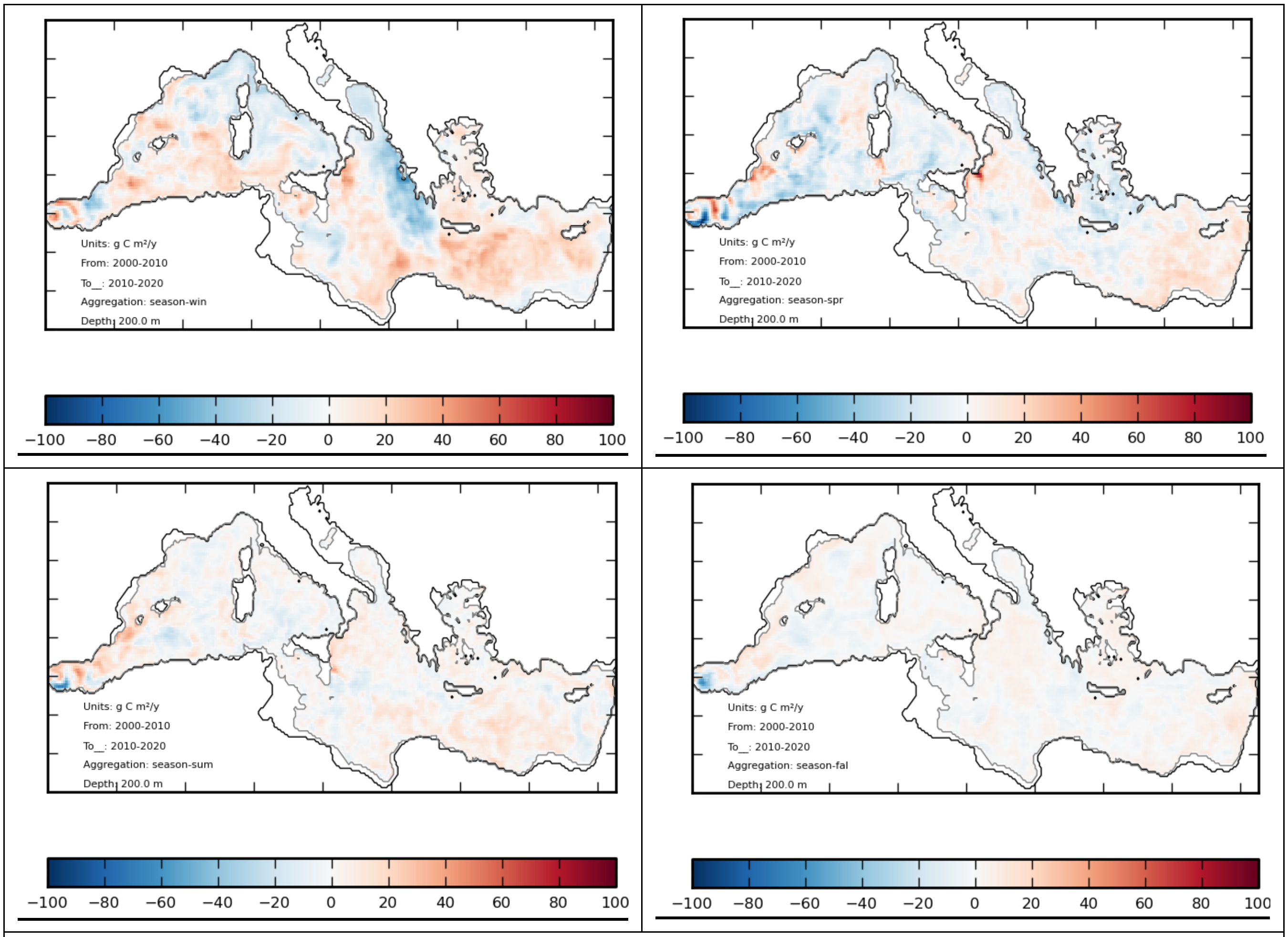

Figure 17. Integrated net primary production over the upper 200 m depth absolute anomalies expressed in gC m^{-2} y^{-1} scenario(2010-2020) – present (2000-2010)). Anomalies are aggregated for the different seasons: Winter (Jan-Feb-Mar) top left, Spring (Apr-May-Jun) top right, Summer (Jul-Aug-Sep) bottom left, Autumn (Oct-Nov-Dec) bottom right.

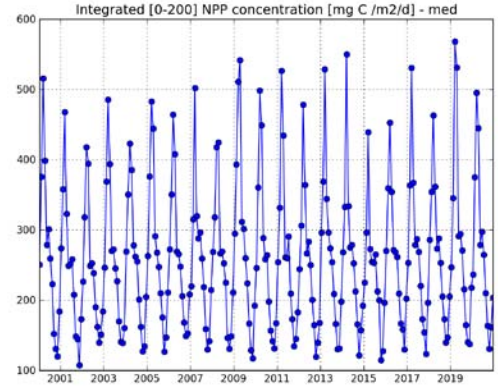

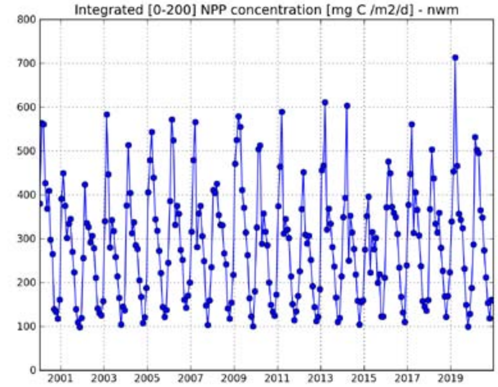

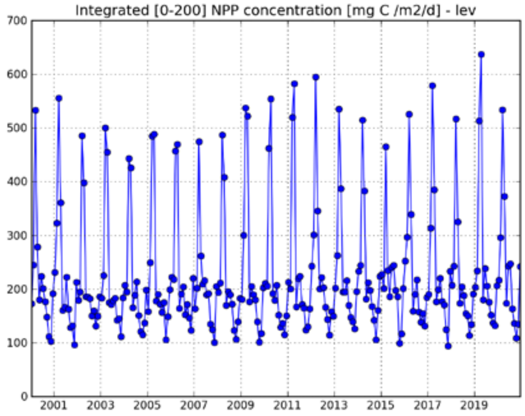

Figure 18. Time series of vertically integrated net primary production (0-200 m) espressed in gC m^{-2} y^{-1} averaged over the entire Mediterranean Sea basin, the western sub-basin and eastern sub –basin.

References

Azov I., 1991. The Mediterranean Sea, a marine desert ?. Mar. Pollut. Bull., 23: 225-232

Adani, M., Dobricic, S., Pinardi, N., 2011. Quality assessment of a 1985–2007 Mediterranean Sea reanalysis.J. Atmos. Oceanic Technol., 28, 569–589 doi:http://dx.doi.org/10.1175/2010JTECHO798.1

Barale, V., Jaquet, J.-M., Ndiaye, M., 2008. Algal blooming patterns and anomalies in the Mediterranean Sea as derived form SeaWiFS dataset (1998-2003). Remote Sens. Environ., 112: 3300-3313

Bandelj, V., Socal, G., Park, Y. S., Lek, S., Coppola, J., Camatti, E., Capuozzo, E., Milani, L., Solidoro, C. (2008). Analysis of multitrophic plankton assemblages in the Lagoon of Venice. Mar. Ecol. Prog. Ser, 368, 23-40.

Bergametti, G., E. Remoudaki, R. Losno, E. Steiner, and B. Chatenet, 1992. Source, transport and deposition of atmospheric phosphorus over the northwestern Mediterranean,. J. Atmos. Chem., 14: 501- 513

Bosc E., Bricaud A., Antoine D., 2004. Seasonal and interannual variability in algal biomass and primary production in the Mediterranean Sea, as derived from 4 years of SeaWiFS observations. Global Biogeochemical Cycles, 18: GB1005

Cornell, S., Randell, A., & Jickells, T. (1995). Atmospheric inputs of dissolved organic nitrogen to the oceans. Nature, 376(6537), 243-246.

Crise, A., Solidoro, C., and Tomini, I., 2003. Preparation of initial conditions for the coupled model OGCM and initial parameters setting. MFSTEP repor t WP11, subtask 11310, 2003,

d'Ortenzio, F., Ribera d'Alcalà, M., 2009. On the trophic regimes of the Mediterranean Sea: a satellite analysis. Biogeoscences, 6: 139-148

Guerzoni, S., Chester, R., Dulac, F., Herut, B., Loÿe-Pilot, M.-D., Measures, C., Migon, C., Molinaroli, E., Moulin, C., Rossini, P., Saydam, C., Soudine, A., Ziveri, P., 1999. The role of atmospheric deposition in the biogeochemistry of the Mediterranean Sea. Prog. Oceanogr., 44 (1-3): 147-190

Herut, B., Krom, M., 1996. Atmospheric input of nutrients and dust to the SE Mediterranean, in The Impact of Desert Dust Across the Mediterranean, edited by S. Guerzoni and R. Chester. Kluwer Acad., Norwell, Mass., pp. 349 – 358

Lazzari, P., Solidoro, C., Ibello, V., Salon, S., Teruzzi, A., Béranger, K., Colella, S., and Crise, A. , 2012: Seasonal and inter-annual variability of plankton chlorophyll and primary production in the Mediterranean Sea: a modelling approach, Biogeosciences, 9, 217-233, doi:10.5194/bg-9-217-2012.

Loÿe-Pilot, M. D., J. M. Martin, and J. Morelli, 1990. Atmospheric input of inorganic nitrogen to the western Mediterranean. Biogeochem., 9: 117-134

Lovato et al., 2013. CMCC Research Papers, RP0207, 1-26

Liu, Y., and R. H. Weisberg (2005), Pattern of ocean current variability on the West Florida Shelf using the Self-Organizing Map, J. Geophys. Res., 110, C06003, doi:10.1029/2004JC002786.

Liu, Y., R. H.Weisberg, and R. He (2006a), Sea surface temperature patterns on the West Florida Shelf using Growing Hierarchical Self-Organizing Maps, J. Atmos. Oceanic Technol., 23(2), 325– 338.

Manca, B., Burca, M., Giorgetti, A., Coatanoan, C., Garcia, M.-J., Iona, A (2004), Physical and biochemical averaged vertical profiles in the Mediterranean regions: an important tool to trace the climatology of water masses and to validate incoming data from operational oceanography, Journal of Marine Systems, Volume 48, Issues 1–4, July 2004, Pages 83–116

Morel, A., Gentili, B., 2009. The dissolved yellow substance and the shades of blue in the Mediterranean Sea. Biogeoscences, 6: 2625-2636

Ribera d'Alcalà M., Civitarese G., Conversano F., Lavezza R., 2003. Nutrient ratios and fluxes hint at overlooked processes in the Mediterranean Sea. Journal of Geophysical Research, 108(C9), 8106, doi:10.1029/2002JC001650

d'Ortenzio, F., Ribera d'Alcalà, M. (2009). On the trophic regimes of the Mediterranean Sea: a satellite analysis. Biogeosciences, 6(2), 139-148.

Siokou-Frangou, I., Christaki, U., Mazzocchi, M. G., Montresor, M., Ribera d'Alcalà, M., Vaqué, D., Zingone, A., 2010. Plankton in the open Mediterranean Sea: a review. Biogeoscences, 7: 1543-1586

Solidoro, C., Bandelj, V., Barbieri, P., Cossarini, G., & Fonda Umani, S. (2007). Understanding dynamic of biogeochemical properties in the northern Adriatic Sea by using self-organizing maps and k-means clustering. Journal of Geophysical Research: Oceans (1978–2012), 112(C7).

Teruzzi, A., S. Dobricic, C. Solidoro, and G. Cossarini (2014), A 3-D variational assimilation scheme in coupled transport-biogeochemical models: Forecast of Mediterranean biogeochemical properties, J. Geophys. Res. Oceans, 119, 200–217, doi:10.1002/2013JC009277.

Turley C.M., Bianchi M., Christaki U., Conan P., Harris J.R.W., Psarra S., Ruddy G., Stutt E.D., Tselepides A., Van Wambeke F., 2000. Relationship between primary producers and bacteria in oligotrophic sea- the Mediterranean and biogeochemical implication. Marine Ecology Progress Series, 193: 11-18

Vilibić, I., Mihanović, H., Šepić, J., & Matijević, S. (2011). Using Self-Organising Maps to investigate long-term changes in deep Adriatic water patterns. Continental Shelf Research, 31(6), 695-711.Volpe et al., 2007

Volpe, G., Santoleri, R., Vellucci, V., Ribera d'Alcalà, M., Marullo, S., D'Ortenzio, F., 2007. The colour of the Mediterranean Sea: Global versus regional bio-optical algorithms evaluation and implication for satellite chlorophyll estimates. Remote Sens. Environ., 107: 625-63

North western Mediterranean (UPS-La)

Methodology

A simulation coupling hydrology and biogeochemistry was done over the period June 2000- June 2013. The hydrodynamic model SYMPHONIE was forced at its lateral boundaries by the NEMOMED8 model described in Herrmann et al., 2010. We use the same atmospheric forcing than this model i.e the ARPERA dataset (Herrmann and Somot, 2008) which is a dynamic downscaling of the ECMWF (European Centre for Medium-Range Weather Forecasts) model reanalysis since 2001. The daily rivers discharges were also realistic for the French rivers and for the Ebro. The biogeochemical model ECO3M-S was previously used to study the Gulf of Lions' pelagic ecosystems impacted by freshwater discharge (Auger et al., 2011) and the pelagic ecosystem dynamics in the offshore areas of the NW Mediterranean basin (Auger et al., 2014). This multi-nutrient and multi-plankton functional types model was forced at the lateral boundaries by the same model that was run at low resolution at the basin scale. The nutrients concentration in the Rhone is fixed from daily measurements. Climatological values are used for the other rivers. The results are presented in the Deliverable 4.12.

Here, the objective is to see the impact of changing nutrients concentration. PERSEUS deliverables 6.2 and 4.6 were used to fix the nutrients under different scenarios. We chose a simple method. First we have calculated the mean annual nutrients discharge for two periods, 2005-2010 and 2015-2020 under 5 scenarios (BAU, REB, RBE, BA and MFA). The results are presented in Table 1 for dissolved inorganic nitrogen and in Table 2 for dissolved inorganic phosphorus. For silicate, the values given in the Deliverable are proportional to the water discharge. A mean increase of the nutrients discharge was calculated between the two periods. We found an increase of 21% for DIN, 24% for silicate and 170% for DIP.

The simulation of Deliverable 4.12 was run with these increases and this simulation was compared to the reference simulation. This procedure allows to directly deduce the impact of rivers changes.

As in Deliverable 4.12, results have been studied in three areas important for the small pelagic fishing activities: the Gulf of Lion, the northern Catalan margin and the southern Catalan margin.

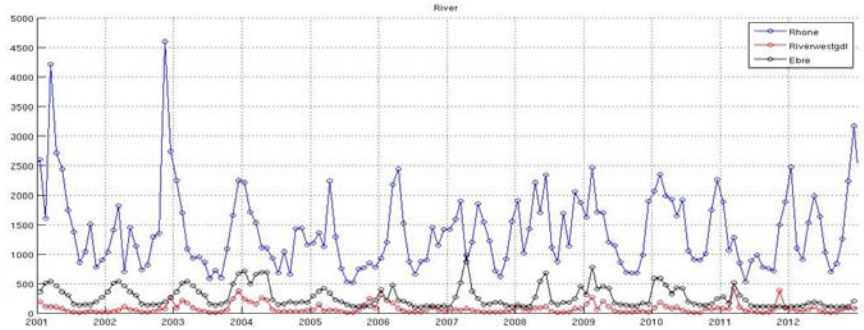

Figure 1 : Monthly averaged rivers discharge in m^3 s^{-1}

The rivers discharge are given on Fig.1 for the Rhône, for the total of the rivers of the western Gulf of Lion and for the Ebro which flows at the boundary between the two Catalan regions (note that for the Ebro, we used climatological values for the three first years). Due to the cyclonic circulation of the region, the Rhone and the rivers of the Gulf of Lion can influence the 3 regions while the Ebro can influence only the two Catalan regions.

Results

Figure 2 presents the change in phytoplankton and zooplankton integrated biomass in the three regions as a function of time. The changes are very low, of the order of 1%, then much lower than the rivers input changes. The most impacted region is the South Catalan for autotrophs and heterotrophs. This is probably because the sources of nutrients outside the rivers are lower for this region (see the new production, Fig.12 Deliverable 4.12). At the opposite, the North Catalan region which is the less impacted region is the region characterized by the highest new production. It is striking that the increases do not correspond to the periods of strong rivers discharges but presents an annual cycle looking like the annual cycle of the biomass. Moreover, the increase presents a “pronounced” interannual variability with low values in 2005 and 2006 (values are always small but the increase varies between 0.6 and 1.5 % for the South Catalan). Then, it seems that, at least in the South Catalan, the period of the bloom is privileged for the ecosystem to have benefit of the increase of rivers input. On the other hand, the low increase in 2005 and 2006 seems related to years with high biomass during the spring bloom (Fig. 5 of Deliverable 4.12) but the relation is not easy to understand. A possibility could be that intense winter conditions could lead to vertical mixing of nutrients and/or low residence time of rivers nutrients on the continental shelf. We will see in the next figure that some compensation also exists between the different groups.

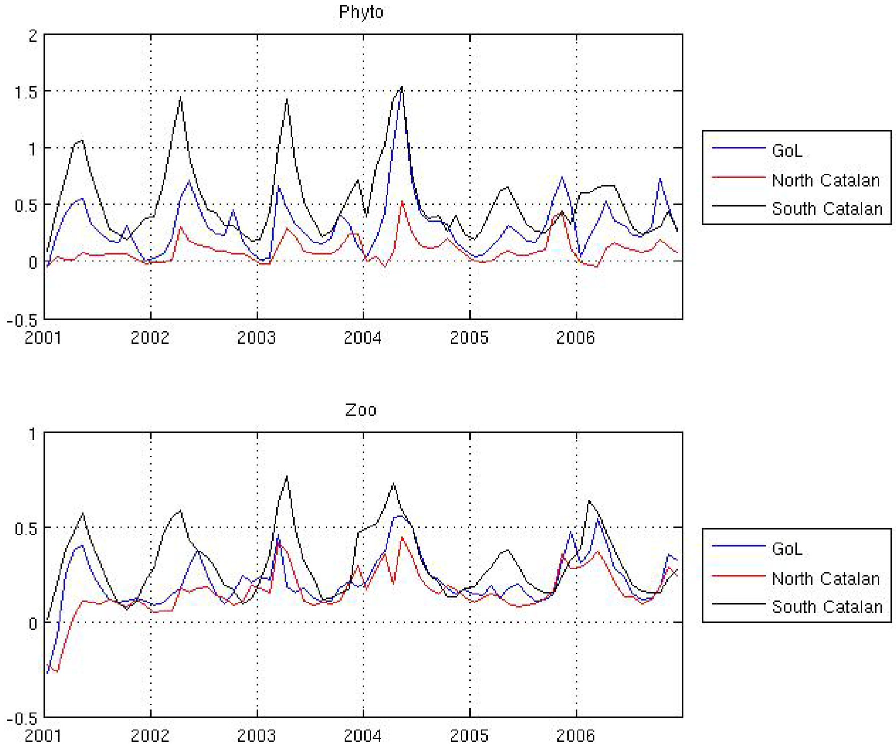

Figure 2: Percent of changes in phytoplankton and zooplankton biomass in the three regions

Figure 3 presents for the South Catalan and the Gulf of Lion regions, the changes in the different phytoplankton and zooplankton groups. Phyto1, phyto2 and phyto3 represent respectively the pico, nano and micro phytoplankton. Zoo1, 2 and 3 represent respectively the nano, micro and meso zooplankton groups. In the South Catalan, the impact can reach 2% for one phytoplankton group. During some priods, the impact on one group can be negative. It is generally the case in winter in the two regions, when nanophytoPk is disadvantaged while microphytoPk is favoured. Even if the impact is low, this is an interesting result as it could indicate an effect of threshold. Nutrients could become enough high to switch (probably locally) the ecosystem from nanoPK to microPk communities. In the Gulf of Lion, this effect is followed one or two months later by a switch from nanozooplankton to microzooplankton.

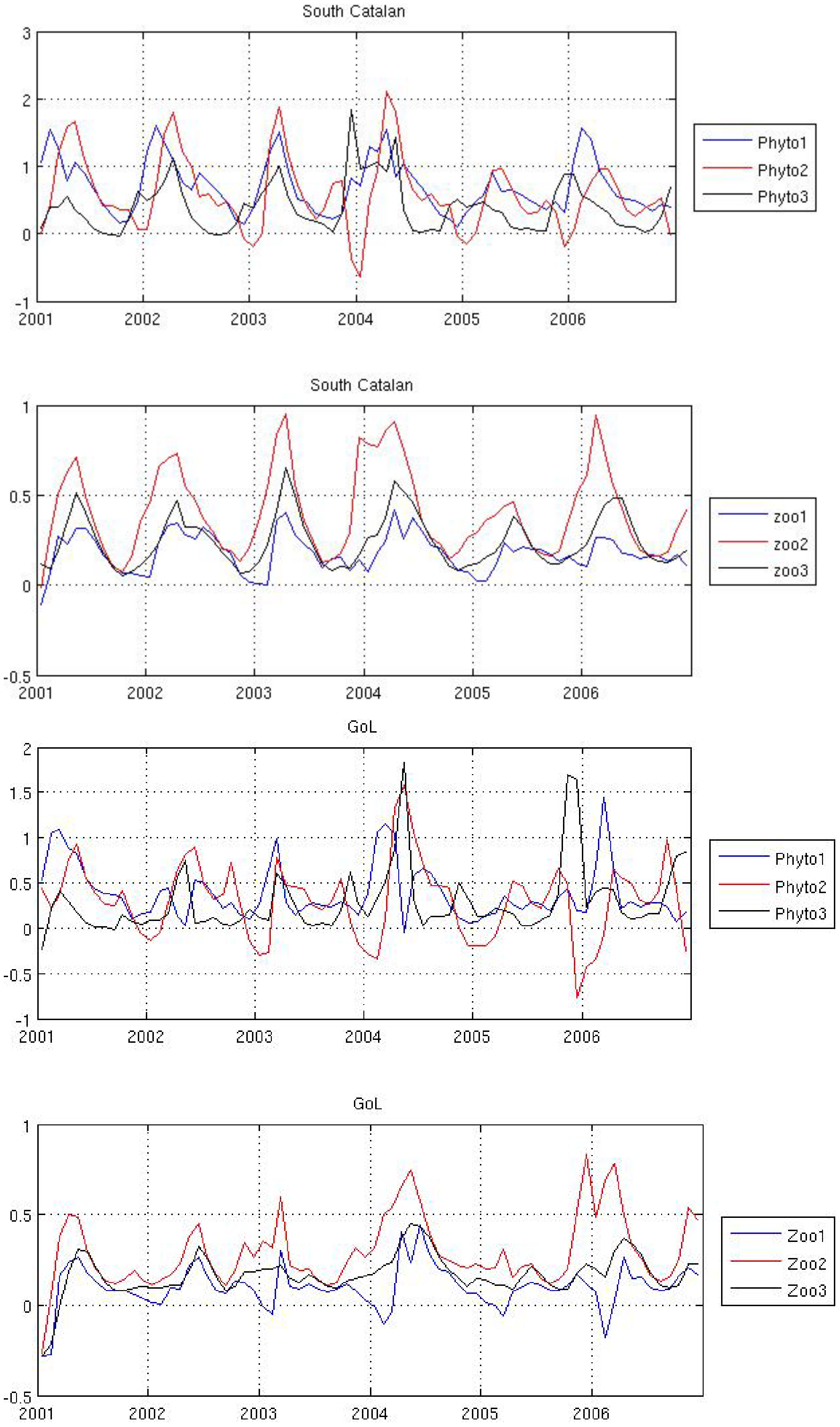

Figure3: Changes in percent in the phytoplankton and zooplankton groups of South Catalan and Gulf of Lion.

Conclusion

The impact of the variation of nutrients between the period 2015-2020 and 2005-2010 is low on the planktonic biomass (< 2%). Three regions have been compared. The South Catalan is the most impacted and the North Catalan the less impacted. This could be related to the fact that the source of nutrients outside the rivers is lower in te South Catalan. We have seen that the impact is stronger during the winter/spring period. It has also been noted that the nutrients changes can induce some shifts in the communities, especially from nanophytoplankton to microphytoplankton and from nanozooplankton to microzooplankton. These shifts are low in intensities at the spatial scale considered here. It is likely that this effect is concentrated in specific areas of the coastal zone.

NAME	moy2005-10	2015-20 BAU	Increase %	2015-20 RBE	Increase %
RHONE	82.81	88.54	6.91	85.70	3.48
VAR	0.54	0.52	-3.12	0.51	-5.93
ORB	0.55	1.10	97.67	1.05	89.83
HERAULT	0.57	0.68	19.03	0.67	17.49
ARGENS	0.86	0.71	-17.62	0.68	-20.72
ARNO	8.38	10.37	23.70	9.75	16.35
AGLY	0.13	0.18	42.36	0.17	36.86
AUDE	2.44	3.14	28.57	3.09	26.52
TET	1.25	1.50	19.31	1.37	8.93
EBRO	19.50	24.03	23.25	22.45	15.12
JUCAR	2.78	3.07	10.26	2.78	-0.28
TOT MEAN	3.70	4.53	24.34	4.25	18.42

NAME	2015-20 REB	Increase %	2015-20 BA	Increase %	2015-20 MFA	Increase %
RHONE	86.85	4.87	87.10	5.17	86.87	4.89
VAR	0.51	-4.91	0.51	-4.98	0.51	-5.06
ORB	1.07	92.49	1.07	93.55	1.07	92.68
HERAULT	0.68	19.33	0.68	19.72	0.68	19.09
ARGENS	0.69	-19.54	0.69	-19.03	0.69	-19.40
ARNO	10.00	19.38	9.94	18.58	9.81	17.02
AGLY	0.17	38.59	0.18	39.40	0.18	38.84
AUDE	3.14	28.62	3.15	29.04	3.14	28.36
TET	1.39	10.77	1.41	12.20	1.40	11.70
EBRO	22.99	17.89	22.91	17.53	22.86	17.24
JUCAR	2.85	2.46	2.85	2.52	2.85	2.27
TOT MEAN	4.35	20.51	4.34	20.85	4.32	20.27

Table 1 : Anual DIN discharge for different rivers averaged over 2005-2010 and over 2015-2020 for the different scenarios.

NAME	moy2005-10	2015-20 BAU	Increase %	2015-20 RBE	Increase %
RHONE	2.37	5.35	126.25	5.12	116.29
VAR	0.01	0.04	663.10	0.04	632.39
ORB	0.02	0.11	433.86	0.11	406.05
HERAULT	0.02	0.05	132.45	0.04	128.20
ARGENS	0.03	0.07	93.46	0.06	81.34
ARNO	0.87	1.47	70.08	1.36	57.15
AGLY	0.01	0.02	32.16	0.01	23.11
AUDE	0.09	0.17	91.63	0.17	87.22
TET	0.11	0.11	1.84	0.09	-10.32
EBRO	0.47	1.39	198.23	1.25	168.13
JUCAR	0.05	0.09	103.91	0.08	71.62
TOT MEAN	0.17	0.35	182.07	0.32	164.49

NAME	2015-20 REB	Increase %	2015-20 BA	Increase %	2015-20 MFA	Increase %
RHONE	5.19	119.42	5.22	120.53	5.20	119.86
VAR	0.04	640.99	0.04	641.99	0.04	641.06
ORB	0.11	413.62	0.11	417.61	0.11	415.15
HERAULT	0.05	131.94	0.05	133.19	0.05	131.93
ARGENS	0.06	84.42	0.06	86.55	0.06	85.61
ARNO	1.40	61.25	1.38	59.99	1.36	57.58
AGLY	0.01	24.96	0.01	26.30	0.01	25.73
AUDE	0.17	90.47	0.17	91.46	0.17	90.42
TET	0.10	-8.57	0.10	-6.82	0.10	-7.31
EBRO	1.28	174.79	1.29	176.22	1.29	175.43
JUCAR	0.08	76.21	0.08	79.44	0.08	78.96
TOT MEAN	0.33	169.01	0.33	170.59	0.33	169.46

Table 2 : Anual DIP discharge for different rivers averaged over 2005-2010 and over 2015-2020 for the different scenarios.

Gulf of Lions HTL model (UnivMED)

The resilience assessment for the Gulf of lion region is reported in deliverables D4.8 (Food web analysis at the regional and basin scale).

Alboran Sea (CSIC)

Abstract

We aimed at analyzing the resilience of the Alboran Sea system using modelling approaches. We analyzed 20 years of data using both an improved coupled physical-biological 3D model and data from other modeling approaches such IBMs. We used a hypothesis-driven approach by which the system would be controlled by the kinetic energy associated to the Atlantic Jet, which has been proposed based on observational studies. The model showed that the larges anomaly in the KE series occurred in 2001, in agreement with observations. The system responded by showing the larges anomaly in nanoplankton vs large phytoplankton biomass particularly during the next year. Our model results suggest a profound change in the LTL levels of the system system in the second half of 2001, that correlated with changes in HTL during approximately one year, which is the approximate time calculated for recovery. Projections were explored using pressure data for 2010-2020, but a lack of spatial resolution and ensemble projections prevented from any quantitative analysis for that time-slice. We performed a scenario-based analysis for different configurations of KE and their impacts on the system's capacity to recover. We generally contend that the system can be severely impacted at LTL and some HTL fractions by transient-short-time phenomena, but that it is unlikely that it is affected at many HTL levels unless a long-time cessation of the AJ occurs.

Introduction

Despite the controversial way to calculate ecosystem's capacity to recover from strong perturbations (usual definition of resilience), the calculation of resilience/resistance continues to be key to understanding human effects on complex natural systems (Hughes et al. 2005). The CSIC team showed within several papers in Perseus, and in their model-derived data in subtasks 4.2.2. and 4.3.3, that the Alboran Sea is a peculiar case within the Mediterranean, for its production and organisation is largely dependent on the Estepona upwelling dynamics in the North Alboran. In this system, we find the effect of winds parallel to the coast and the inflowing Atlantic Jet to drive production in the area (with the obvious overlying seasonal signal), producing total production estimates that surpass many other areas in the Mediterranean. This system is rarely disrupted but in the documented cases when it is, the cessation of the Atlantic Jet provokes not only changes in the distribution of the production but in the relative proportion of producers (See Subtask 4.3.3.). We proved that this disruption is detectable through modelling in primary and secondary producers, and both modelling data (Catalán et al., 2013) and observational data (Ruiz et al., 2013) showed that this is in accordance to major changes in HTL such as anchovy populations. Most importantly, the "change of phase" of the system may not always have detrimental effects. For example, the disruption of the 2001 Jet in the last part of the year released the potential of anchovy populations, which expanded in the area. It is, therefore, assumable that the resilience of such a system can be calculated as the time it takes the main driving agent in the area (the Atlantic Jet) to recover from a disruption. As a first step, we explored in subtask 4.2.2. a model-derived proxy to trace the system's state. The Kinetic energy derived from the model (and as expected from altimetry), resulted in a reasonable predictor of the system's production (Fig.1). Due tot he fact that in our model all biological components depend on production (See subtask 4.2.2.), it is expected that (due to model constraints) a failure in production will cascade down provoking alterations in all the system. Therefore, we concentrate this contribution in the search for clear alteration patterns and the exploration of how the system recovers from them. No ad-hoc disruptions were provoked because a natural disruption was well captured by the model (see CSIC contribution to 4.3.3.)

Material and Methods

Our results on model-based resilience cannot be analyzed for the different time-slices, because disturbance typically occurs sporadically. In our model, we did not provoke disturbances on purpose but relied on the observation that a major disturbance was observed in 2001 (Ruiz et al., 2013). Based on the model-derived relationships between production and kinetic energy of the system (Fig. 1), and having analysed the response of the system during two decades by using Perseus-generated models (see subtask 4.3.3.), we will explore the resilience of the system assuming that primary production will only be indicative of changes in the system if both compartments of primary production are altered. We will assume that, being this a relatively simple system dominated through an upwelling, we should observe a relative alteration of the energy in the system as well. We will concentrate on the beginning of the 2000s, a period when a massive cessation of the AJ occurred with profound ecological effects (Mercado et al. 2007, Ruiz et al. 2013). Also, our model gave significant organizative alterations (subtask 4.3.3.). The monthly anomalies and filtered values of the average Kinetic energy in two spatial scales (North Alboran and All Alboran) were explored for averaged values at 100 m, whereas the production was integrated over 100 m, following the reasoning of contributions 4.3.3. and 4.2.2.

We calculated monthly anomalies and took average anomaly values for the first and second half of each year. This accounts for the periods of peak production and stabilisation of the column (first half) and disruption of the system through physical enthropy owing to thermocline disruption (second half). By substracting the two, we inspected peculiar years with respect to production dynamics.

The MS (magnitude that puts the system into an alternate state) and the RT (recovery time, which puts the system back to usual values) were aimed as the main variables to be calculated, and the ratio (MS/RT) was the magnitude to depict resilience according to the general literature (Fig.2). One essential assumption was that the organization in the previous 5 years to year 2001 were within normal values with respect to several ecosystem components at least in the pelagic realm, which is partially supported by observations in Mercado et al (2007) and Ruiz et al (2013). This phenomenological study (based on abrupt alterations) cannot be adequately extrapolated in the future. For this reason, it does not make sense to make empirical predictions in the future to 2020, but to make scenario analysis. We therefore assumed scenarios of increasing or decreasing KE annual values and how this might affect the resilience of the system. Further, the ideal predictors for KE should be an ensemble models including both low-frequency metorological oscillations and local-based wind data, which are not available at the moment. We did explore the pressure data provided by M.Vichi, but found them difficult to relate to our data due to resolution problems.

Results

Resilience before 2010

Our model-based results showed that a major alteration was observed in 2001, in agreement with observational data. The use of half-year differences in averaged monthly anomalies indicated that when the whole domain was considered, the following features were observed (Fig.3):

1) The largest peak in KE (anomalies) differences was observed in 2001. This was interpreted as a combination of large kinetic energy values during the first half of the year and low KE anomalies during the second part of the year (see subtask 4.2.2.).

2) An initial high production of large phytoplankton occurred at the beginning of the year concurrently with high kinetic energy in spring. However, the lowest large-phytoplankton peak (negative difference) was observed in 2002, indicating a potential change in the system by the end of 2001.

3)The lowest peak in nanophytoplankton (difference between first and second half of the year) was observed in 2001, which indicates that large amounts of small phytoplankton related to non-upwelling conditions were present in the area in the second half.

The MS was difficult to calculate because it was a combination of systems what affected the Alboran Sea. On average, the magnitude of the change in the energy of the system at the end of 2001 was ca. 50% lower than in any other year of the series until 2005 (Ruiz et al., 2013). Based only on the direct observable outputs of our model, at least the LTL was recovered in less than one year, in direct relation to the re-installation of the jet. Consequences for the fisheries lasted also 1 year (see Discussion) and resumed afterwards.

Projecting Resilience

The exercise of projecting resilience was unfruitful using the pressure data provided in WP4 due to several factors. Firstly, probably the resolution was not adequate to depict the fine-scale wind forcing over the jet provoked by pressure changes. Second, NAO has been previously related to the AJ (Ruiz et al., 2013) but projecting NAO at the short time makes no sense when abrupt changes are to be detected, and it also needs from an ensemble model to search for uncertainty in the estimations.

An exercise on the potential effects of the AJ changes on the resilience are depicted in Table 1. Due to the nature of the persistence in pressure changes it is unlikely that permanent disruptions of the jet occur (as the historical record shows). However, if they occur, the potential recovery times may depend on the duration and magnitude of the disruptions. Clearly, strong long-lasting disruptions might provoke changes in a higher number of components of the system, On the contrary, at the scale of months of affection and recovery, consequences are moderate, as we observe values in LTL and HTL back to normal during next year.

Discussion

We could observe, through the model, the ecosystem's disruption in 2001. Our results agree very well with the system's dynamics as inferred through satellite observation, which showed that the second half of 2001 was an extremely stable period with an almost absent AJ from october (see last figure in subtask 4.3.3.).

The sistem, being controlled by a define forcing, could recover aproximately at the same time that the AJ was restabished in 2002. Resilience could not be quantified in a systematic way as only one disruption was observed. In the future, it would be desirable to perform a series of forced disruptions to evaluate the change in components of the system. However, it was first to be proven that the model could capture the observed changes.

In the absence of other data on higher trophic levels to calculate resilience within the sale coupled model, we used model's data from (Catalán et al. 2013) and observational data from Ruiz et al., (2013). Ruiz et al. (2013) observed that at least part of the HTL levels were severely disrupted following the AJ modification by the last quarter of 2001. The catches od anchovy increased dramatically during that year and the beginning of 2002, due to a change in predatory fields and an enlarged "vertically stable" and productive (though less in absolute values) area. After the disruption, the model suggests that the system recovered. However, although we do have satellite data resolving several phytoplnkton groups, these data do not encompass the 2011 event, and therefore they could not be used to explore the disruption. We contend that this system can recver quickly is the perturbations is profound and lasts less than one year (Table 1). however, further modelling and observational studies need to be conducted to provide more accurate insight into the resilience of the system.

Table 1.

Potential scenarios for 2010-2020 with respect to resilience in case that abrupt anomalies with respect to KE occur. + and - indicate magnitude in qualitative terms.

Direction of KE change	KE rate of change and recovery	Consequences for primary production	Consequences for organization	Consequences for HTL (probability of affecting a larger number of components
Increase	Abrupt	Increase +	stable+	low to moderate
Increase	Sustained	increase ++	stable++	high
Decrease	Abrupt	Decrease--	change++	moderate
Decrease	Sustained	Decrease-	change+	high

Figures

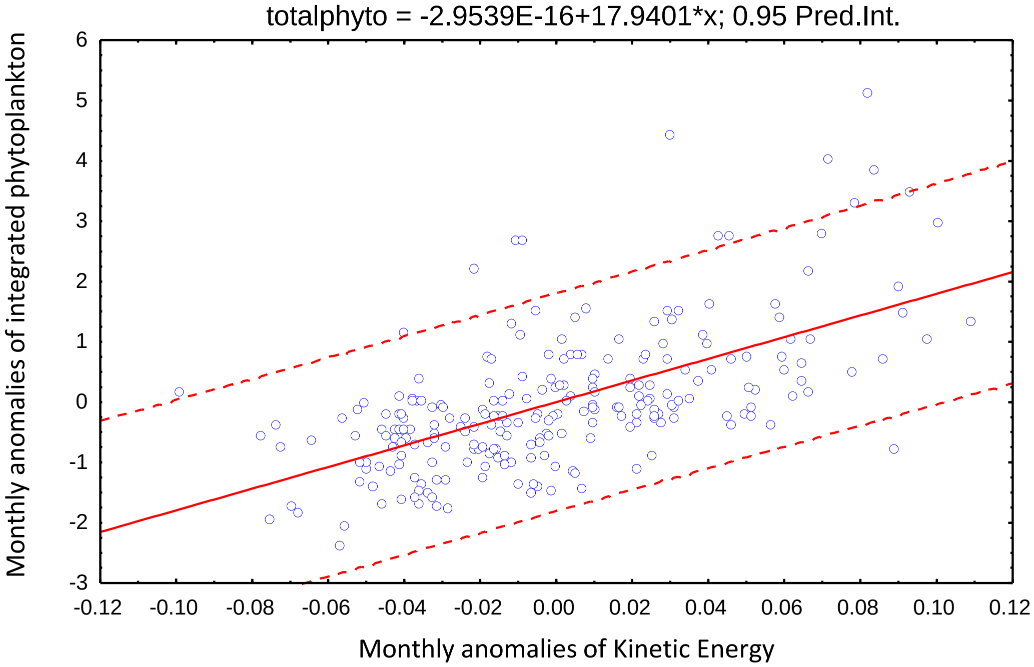

Fig. 1. Regression and 95% prediction intervals between the monthly anomalies of kinetic energy of the North Alboran (average in the first 10 m) and the anomalies in total phytoplankton biomass in the same area and integrated over 10 m.

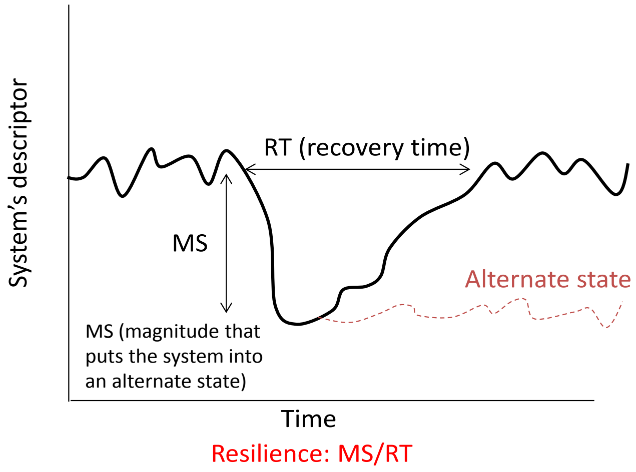

Fig.2. General frame to explore resilience properties of the Alboran Sea. In System's descriptor we use kinetic energy.

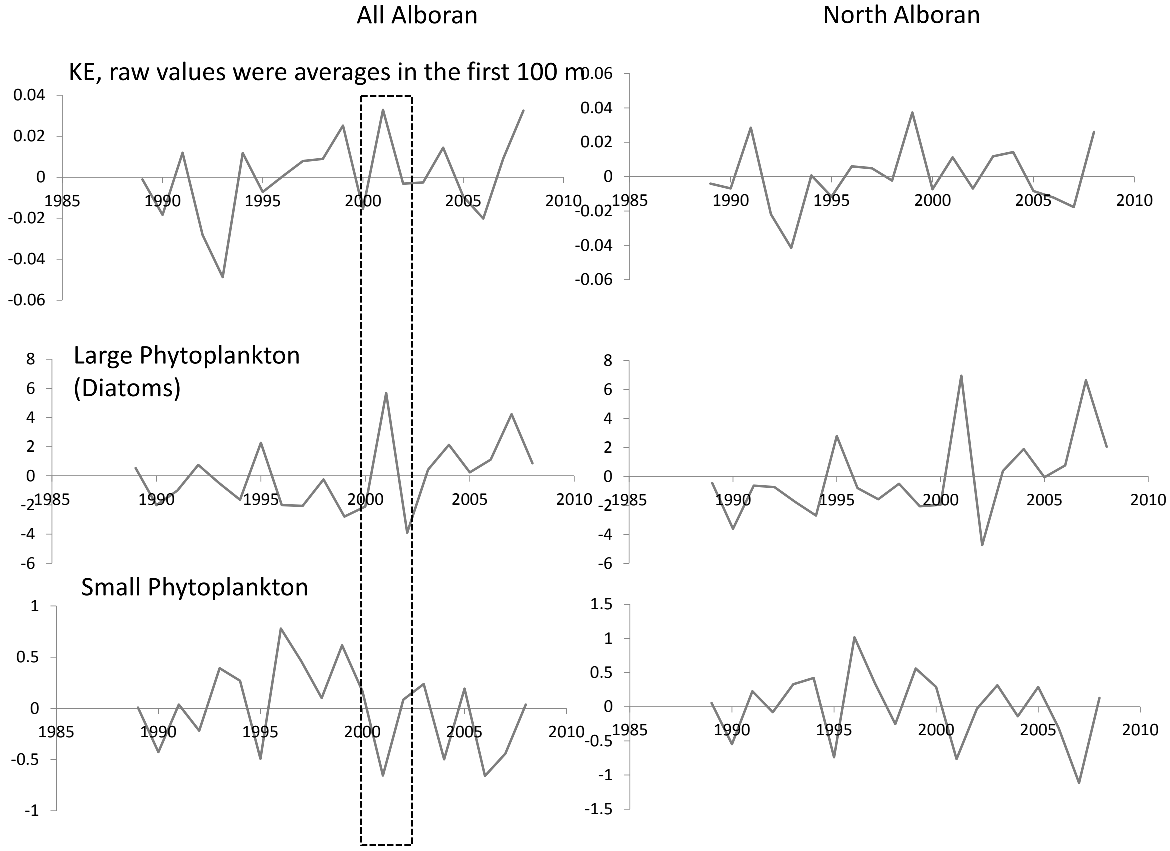

Fig.3. Differences of averaged anomalies during the first and second half of the year.

References

Catalán, I. A., D. Macías, J. Solé, A. Ospina-Álvarez, and J. Ruiz. 2013. Stay off the motorway: resolving the pre-recruitment life history dynamics of the European anchovy in the SW Mediterranean through a spatially-explicit individual-based model (SEIBM). Progress in Oceanography **111**:140-153.

Hughes, T. P., D. R. Bellwood, C. Folke, R. S. Steneck, and J. Wilson. 2005. New paradigms for supporting the resilience of marine ecosystems. Trends in Ecology and Evolution **20**:380-386.

Mercado, J. M., D. Cortés, A. García, and T. Ramírez. 2007. Seasonal and inter-annual changes in the planktonic communities of the northwest Alboran Sea (Mediterranean Sea). Progress in Oceanography **74**:273-293.

Ruiz, J., D. Macías, M. M. Rincón, A. Pascual, I. A. Catalán, and G. Navarro. 2013. Recruiting at the Edge: Kinetic Energy Inhibits Anchovy Populations in the Western Mediterranean. PLoS ONE **8**.

Northern Aegean Sea HTL model (HCMR)

Introduction

The Marine Strategy Framework Directive (MSFD; EU, 2008) establishes "a framework within which Member States shall take the necessary measures to achieve or maintain good environmental status in the marine environment by the year 2020 at the latest". One of the ecosystem attributes that has been proposed to characterize the "health" of the marine ecosystem is resilience (Costanza and Mageau, 1999). Resilience can be assessed by measuring the changes of ecosystem structure and functioning caused by different stresses or environmental and management scenarios.

Ecosystem modelling integrates available information to study direct and indirect trophic interactions among ecosystem compartments, including fishing activities and the environment. It is therefore a useful tool for fisheries management (Christensen and Walters 2004). The broad use of the trophic modelling tool "Ecopath with Ecosim (EwE)" (Christensen and Walters 2004) has contributed to complement previous knowledge of the structure and functioning of marine ecosystems and has enabled the proposal of ecological indicators and reference limits based on model outputs and meta-analysis of models' results (e.g., Christensen, 1995; Libralato *et al.*, 2008; Heymans *et al.,* 2014; Lynam and Mackinson, 2015).

In the current work we used an end-to-end model built for the North Aegean Sea (NAS) ecosystem to simulate a series of nutrient load (related to river runoffs) and fisheries scenarios. Several ecosystem indices and biomasses of the functional groups were estimated for each simulation. Resilience was assessed by comparing the output of each scenario with the business-as-usual (BAU) scenario.

Methods

The coupled NAS model

The end-to-end NAS model area is defined by the 20 m and 300 m isobaths (Figure 1) covering 8374 km^2 in total. This is mainly the area where trawlers, purse seiners and the biggest fraction of artisanal fleets operate.

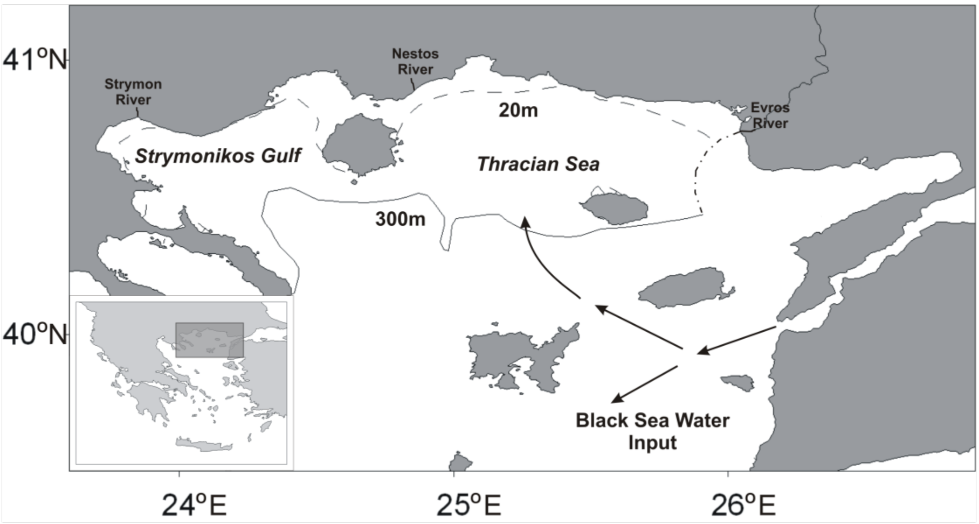

Figure 1. North Aegean Sea (Strymonikos Gulf and Thracian Sea). Isobaths of 20m and 300m which define the model area are shown, as well as the most important rivers of the area. Arrows indicate the direction of Black Sea Water Input.

The structure and the methodology used to build the NAS en-to-end model is described in detail in PERSEUS D4.4 and D4.8. Outputs of the OPATB-BFM LTL (Lazzari *et al*. 2012) were used as input for the biomasses and diet matrix of the LTL groups as well as to drive the LTL components of the model. Flows and biomasses of the model are expressed in phosphorus, P, which is considered the limiting nutrient in the Mediterranean.

The HTL model is based on the previously developed Ecopath model in the area for the period 2003-2006 (Tsagarakis *et al.*, 2010) which was adjusted to input data from the early 1990s. This model followed a standardized structure which was agreed for all the Mediterranean areas (Gulf of Lions, Adriatic, NAS) and which is described in detail in PERSEUS D4.4. The structure of the food web of the coupled model is shown in Figure 2. For the coupling between LTL and HTL components of the model we followed the methodology described in Libralato and Solidoro (2009). The model simulated the period 1993-2020 using forcing function from LTL input from the BFM (bacteria, pico- and phytoplankton) and time series of fishing effort data. The coupled model was then fitted to LTL and HTL data for the period 1993-2010. For the period 1993-2000, no input from the OPATM-BFM was available thus forcing was based on time series constructed based on climatology using data from the 2000-2010 period.

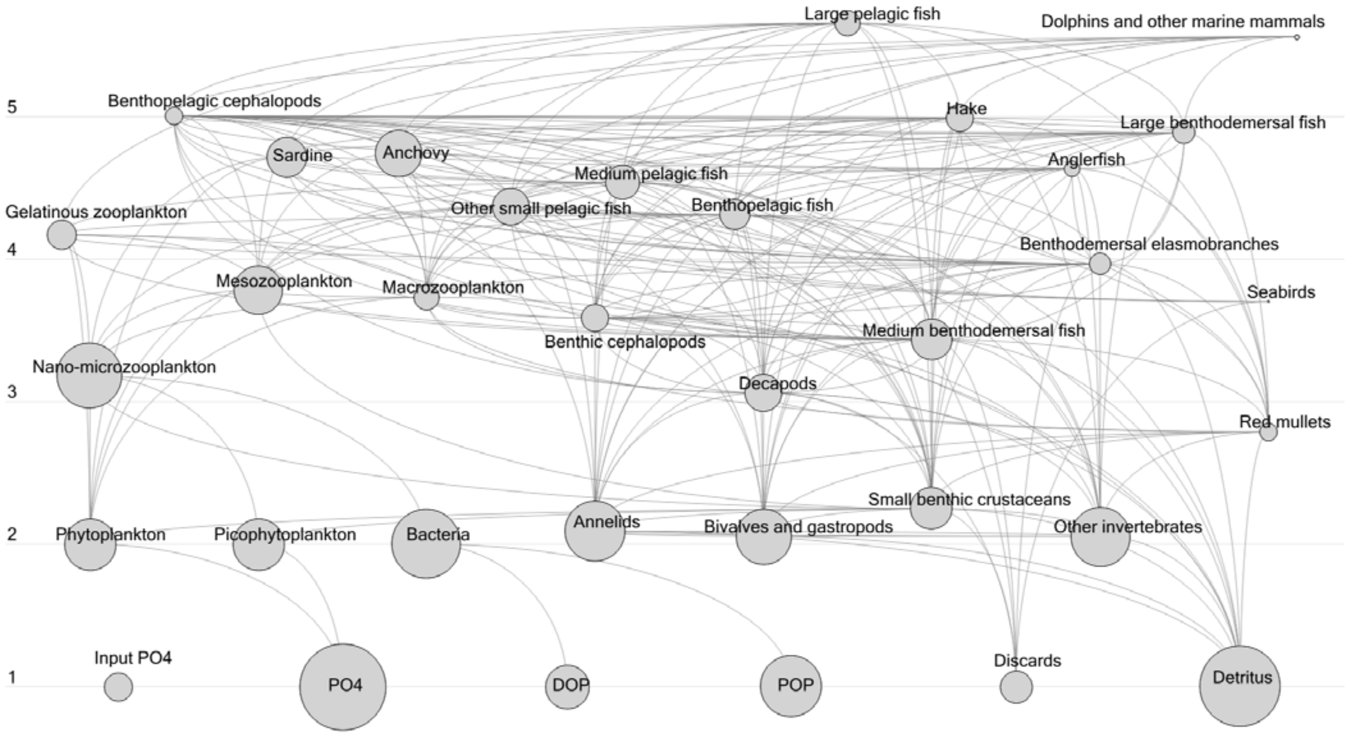

Figure 2. Structure of the foodweb of the end-to-end NAS model. The links between the different compartments show the trophic flows.

Scenarios

The OPATB-BFM LTL simulation used for the end-to-end NAS model were performed using nutrient river run-off scenarios from D4.6 (BAU, BA, MFA, REB, RBE) for the period 2011-2020 which are described in Table 1. Results of the models using BA, MFA, REB, RBE data were compared to those of the model using BAU (business as usual) scenario considered as the reference one for the period 2011-2020. In all these LTL scenarios fishing pressure was considered constant between 2010 and 2020.

A series of fisheries related (affecting HTL) simulations were explored which used BAU scenario data for LTL. These included decreases/increases of the fishing effort of specific or all gears or changes in the fishing mortality of some functional groups(Table 2). Results of the models using the different fisheries scenarios were compared to those of the model using BAU and constant fishing effort between 2010 and 2020 (BAU). A series of ecosystem metrics (Table 3) were estimated or extracted from the NAS coupled model and were used to compare among nutrient load and fisheries scenarios. Each of these metrics can be considered to be mainly related to one of the ecosystem attributes (Vigor, Organisation, Resilience, Exploitation) but the difference among scenarios was also considered as a measure of the system's resilience.

Table 1. Low trophic level model scenarios used in this report (from PERSEUS Deliverable 4.6)

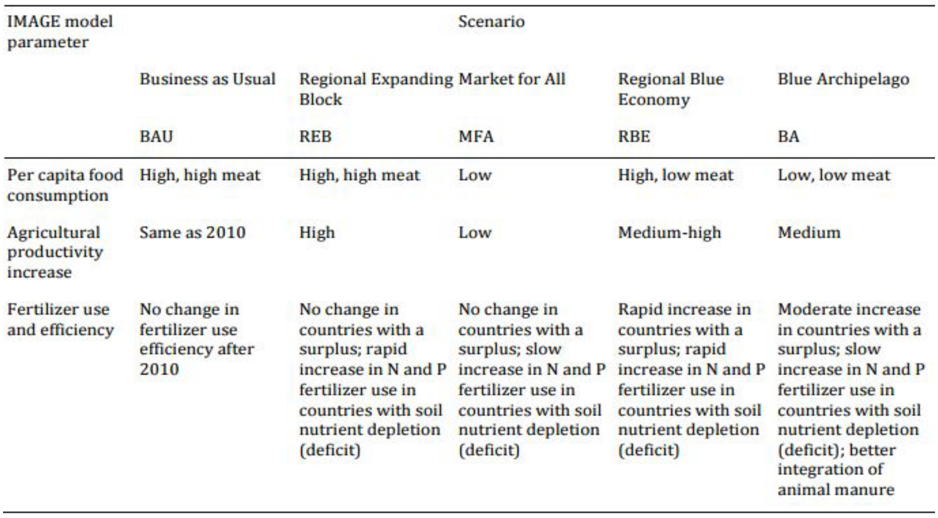

IMAGE model parameter	Scenario				
	Business as Usual	Regional Expanding Block	Market for All	Regional Blue Economy	Blue Archipelago
	BAU	REB	MFA	RBE	BA
Per capita food consumption	High, high meat	High, high meat	Low	High, low meat	Low, low meat
Agricultural productivity increase	Same as 2010	High	Low	Medium-high	Medium
Fertilizer use and efficiency	No change in fertilizer use efficiency after 2010	No change in countries with a surplus; rapid increase in N and P fertilizer use in countries with soil nutrient depletion (deficit)	No change in countries with a surplus; slow increase in N and P fertilizer use in countries with soil nutrient depletion (deficit)	Rapid increase in countries with a surplus; rapid increase in N and P fertilizer use in countries with soil nutrient depletion (deficit)	Moderate increase in countries with a surplus; slow increase in N and P fertilizer use in countries with soil nutrient depletion (deficit); better integration of animal manure

Table 2. High trophic level model scenarios related to fisheries used in this report.

Code	Scenario
P10All	Increase by 10% the fishing effort in term of number of boats for all the fleets for the period 2010-2020 compared to 2009
M10All	Decrease by 10% the fishing effort in term of number of boats for all the fleets for the period 2010-2020 compared to 2009
P10Btwl	Increase by 10% the fishing effort in term of number of boats for the benthic trawls for the period 2010-2020 compared to 2009
M10Btwl	Decrease by 10% the fishing effort in term of number of boats for the benthic trawls for the period 2010-2020 compared to 2009
P10SPF	Increase by 10% the fishing mortality for commercial small pelagic fish species (sardine and anchovy) for the period 2010-2020 compared to 2009
M10SPF	Decrease by 10% the fishing mortality for commercial small pelagic fish species (sardine and anchovy) for the period 2010-2020 compared to 2009
P10LPF	Increase by 10% the fishing mortality for large pelagic fish species for the period 2010-2020 compared to 2009
M10LPF	Decrease by 10% the fishing mortality for large pelagic fish species for the period 2010-2020 compared to 2009

Table 3. Metrics used to compare the "health" (vigor, organization and resilience) over the time and between of the marine systems Costanza and Mageau (1999)

Attribute	**Metric**
Vigor	NPP (net primary production) T (Throughput) Catch (total catch)
Organisation	K's Q (Kempton's Q) FiB (Fishing in Balance) AMI (Average Mutual Information) A (Ascendency) FCI (Finn's Cycling Index) mPL (Mean Path length)
Resilience	H-AMI (Entropy - Average Mutual Information) = [(Capacity-Ascencency) / Throughput] SfG (Scope for Growth = Total production – Total primary production)
Exploitation	C/B (catch over biomass) TLc (trophic level of the catch)

Results

Trends of metrics were estimated for all the scenarios for the hindcast and forecast period. An example of estimated time series is given in Figure 3 for the total catch. Then the values of the metrics for year 2020 were compared for each scenario in relation to BAU and the results are presented in Table 4 as relative (%) change. Compared to BAU scenario seven (NPP, T, AMI, A, mPL, H-AMI, TLc) out of 13 indices showed no or little (<|5%|) change in the four nutrient load and the eight fisheries scenarios. C/B ratio changed substantially only in the scenarios where the fishing effort increased/decreased by 10% for all gears (Table 4) while SfG decreased substantially only in three of the nutrient load scenarios (MFA, REB, RBE). The outputs of these three scenarios showed also reduction in Catch, Kempton's Q diversity and FCI while increases were observed for the Fishing in Balance index. However the majority of changes were not very high and only the three indices related to organization (K's Q, FiB and FCI) changed by more than 10%. In general, the fisheries scenarios affected less the ecosystem compared to the nutrient load scenarios as evidenced by the % changes in the metrics mentioned above. The indices that were affected at the fisheries scenarios were mainly the ones related to fisheries yield and the balance of the fisheries (Table 4).

The conclusion that nutrient load scenarios affected more than the fisheries related ones is further supported by the simulated changes in biomass per functional group (FG). Even though no substantial changes were observed in the lowest FGs (phytoplankton, bacteria, nano- & micro-zooplankton) for any of the scenarios, the changes were transferred up the food web (Table 5). In the nutrient load scenarios changes were observed for almost all FGs; specifically, biomasses generally decreased in MFA, RBE and REB scenarios and increased in BA scenario. As concerns fisheries changes, increased biomasses followed reductions in fishing effort/mortality and the opposite for increases. Opposite patterns were observed only in cases that a prey FG was favoured by e.g. increased fishing pressure on its predator (for example the increase in the mortality of large pelagic fish resulted in relaxation of the predation mortality of benthopelagic cephalopods and increase in their biomass; Table 5).

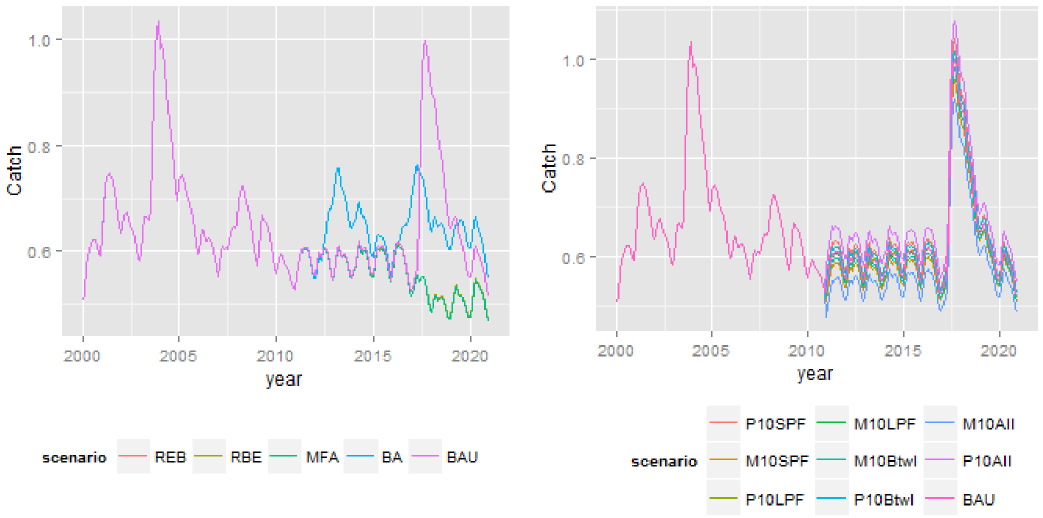

Figure 3. Estimates of total Catch under different nutrient load (left) and fisheries (right) scenarios. The 2000-2010 period corresponds to the coupled model fitted to data and the 2011-2020 to the scenario data.

Table 4. Comparison of indices under different LTL and HTL scenarios of the North Aegean Sea. Absolute values are presented for the BAU scenarios for year 2020, while relative changes (%) are reported for the remaining scenarios. Significant differences (> |5%|) between BAU and all other scenarios are indicated in bold and in shaded cells (red for lower values and green for higher values compared to BAU). The indices are grouped according to the attribute (vigor, organization, resilience and exploitation) that they are mainly related to.

metrics	**Vigor**			**Organisation**						**Resilience**		**Exploitation**	
	NPP	**T**	**Catch**	**K's Q**	**FiB**	**AMI**	**A**	**FCI**	**mPL**	**H-AMI**	**SfG**	**C/B**	**TLc**
BAU in 2020	1.17	1258.75	0.56	7.13	-0.0004	1.99	2494.60	56.72	10.59	2.64	305.86	0.0043	3.75
Nutrient load scenarios													
BA-BAU	1.27	0.53	**7.09**	-4.43	**-23.76**	0.31	0.84	-0.26	-1.08	0.33	0.76	4.34	0.12
MFA-BAU	-1.93	-3.48	**-9.36**	**-27.39**	**14.41**	0.51	-2.92	**-33.40**	3.29	-1.88	**-6.58**	2.62	-0.69
RBE-BAU	-1.89	-2.98	**-8.76**	**-27.06**	**12.20**	0.45	-2.47	**-26.85**	2.24	-1.79	**-5.70**	2.70	-0.59
REB-BAU	-1.86	-3.13	**-8.84**	**-27.25**	**12.35**	0.49	-2.59	**-39.33**	2.46	-1.80	**-5.98**	2.75	-0.60
Fisheries scenarios													
p10All-BAU	-0.03	-0.03	**5.94**	3.06	**-21.34**	0.01	-0.02	**-9.21**	-0.20	-0.07	-0.09	**6.38**	-0.28
m10All-BAU	0.03	0.03	**-6.24**	**-5.37**	**19.30**	0.07	0.10	0.09	0.23	0.01	0.10	**-6.68**	0.32
p10Btwl-BAU	0.00	0.00	1.65	0.27	-4.72	-0.01	-0.01	0.00	-0.05	0.00	-0.02	1.73	-0.07
m10Btwl-BAU	0.01	0.00	-1.68	-0.34	4.62	0.01	0.02	0.00	0.05	0.00	0.02	-1.77	0.08
p10SPF-BAU	-0.02	-0.02	2.13	-0.26	**-9.43**	-0.04	-0.06	0.00	-0.13	-0.01	-0.06	2.46	-0.06
m10SPF-BAU	0.02	0.02	-2.26	0.25	**8.78**	0.04	0.07	0.01	0.14	0.01	0.07	-2.59	0.07
p10LPF-BAU	0.00	0.00	-0.19	1.26	-0.15	0.00	0.00	0.05	-0.05	0.00	0.00	-0.13	-0.07
m10LPF-BAU	0.00	-0.01	0.14	-1.46	0.19	0.00	0.00	-0.05	0.07	0.00	0.00	0.07	0.06

Table 5. Comparison of the FGs' biomasses under different LTL and HTL scenarios. Absolute values (mg P* m^{-2}) are presented for the BAU scenarios for year 2020, while relative changes (%) are reported for the remaining scenarios. Significant differences (> |5%|) between BAU and all other scenarios are indicated in bold and in shaded cells (red for lower values and green for higher values compared to BAU)

	Nutrient load scenarios					**Fisheries scenarios**							
Functional group	**BAU**	**BA**	**MFA**	**RBE**	**REB**	**P10all**	**M10all**	**P10Btw**	**M10Btw**	**P10SPF**	**M10SPF**	**P10LPF**	**M10LPF**
Phytoplankton	6.63	3.09	-4.41	-4.03	-4.16	-0.07	0.08	-0.01	0.01	-0.05	0.05	0.00	0.00
Picophytoplankton	7.60	-0.12	-2.49	-1.84	-1.88	-0.02	0.02	0.00	0.00	-0.02	0.02	0.00	0.00
Bacteria	34.09	0.80	-0.71	-0.69	-0.70	-0.02	0.02	0.00	0.00	-0.01	0.01	0.00	0.00
Nano-microzooplankton	21.94	0.63	-4.19	-3.33	-3.44	-0.05	0.06	-0.01	0.01	-0.04	0.04	0.00	0.00
Mesozooplankton	4.34	**7.17**	**-8.73**	**-7.71**	**-7.90**	-0.15	0.17	-0.02	0.03	-0.10	0.11	0.00	0.00
Macrozooplankton	0.60	0.88	1.66	2.08	2.02	-0.47	0.57	0.04	-0.03	0.00	0.00	-0.28	0.31
Gelatinous zooplankton	0.74	**13.68**	**-6.60**	**-5.59**	**-5.75**	0.64	-0.68	0.04	-0.04	-0.12	0.12	0.09	-0.10
Annelids	14.52	**5.69**	**-5.95**	**-5.48**	**-5.56**	0.10	-0.07	0.12	-0.12	-0.13	0.14	0.01	-0.03
Bivalves and gastropods	6.85	1.31	**-44.35**	**-43.69**	**-43.92**	-0.91	1.07	-0.11	0.12	-0.76	0.80	0.17	-0.17
Benthic cephalopods	0.53	-2.91	**-50.57**	**-49.98**	**-50.19**	**-7.02**	**7.64**	-0.93	0.92	-0.86	0.92	0.12	-0.11
Benthopelagic cephalopods	0.21	**11.25**	**-16.17**	**-15.38**	**-15.54**	4.08	**-5.87**	-0.77	0.77	0.13	-0.20	**9.64**	**-10.30**
Small benthic crustaceans	3.15	1.97	**10.02**	**10.16**	**10.19**	1.16	-1.21	0.20	-0.19	0.00	0.00	0.07	-0.10
Decapods	2.02	**7.66**	**14.41**	**14.45**	**14.50**	3.01	-3.01	0.51	-0.48	-0.03	0.03	0.46	-0.53
Other invertebrates	13.98	0.79	**-47.89**	**-47.18**	**-47.44**	-0.21	0.11	-0.22	0.22	-0.69	0.73	-0.12	0.15
Sardine	2.23	**15.12**	-1.94	-1.30	-1.40	-3.74	4.40	0.01	-0.01	-4.62	**5.06**	-0.88	1.09
Anchovy	4.20	**16.44**	**6.02**	**6.63**	**6.56**	1.41	-1.97	-0.04	0.04	-1.39	1.36	1.67	-2.15
Other small pelagic fish	1.73	**8.65**	**-8.71**	**-8.13**	**-8.23**	-0.46	0.48	0.19	-0.18	0.36	-0.37	1.24	-1.20
Medium pelagic fish	1.46	**7.93**	**-7.34**	**-6.86**	**-6.94**	**-7.53**	**8.89**	-0.67	0.67	0.08	-0.07	-0.51	0.71
Benthopelagic fish	1.12	**6.19**	**-19.19**	**-18.47**	**-18.63**	1.13	-1.25	-0.06	0.02	-0.02	0.02	-0.12	0.12
Large pelagic fish	0.80	-0.07	**-39.96**	**-39.42**	**-39.63**	**-22.33**	**27.63**	-0.89	0.90	**-5.14**	**5.52**	**-18.65**	**22.35**
Red mullets	0.31	**7.66**	**10.65**	**10.77**	**10.79**	-2.02	2.19	-1.00	1.01	0.10	-0.10	-0.61	0.67
Medium benthodemersal fish	3.11	1.19	**-22.58**	**-22.11**	**-22.25**	-2.71	2.80	-0.59	0.57	-0.25	0.27	-0.74	0.85
Hake	1.08	-1.72	**-15.43**	**-15.13**	**-15.22**	**-5.05**	**5.21**	-2.75	2.79	-0.66	0.68	0.40	-0.44
Anglerfish	0.03	**15.94**	**-59.41**	**-58.84**	**-59.10**	**-23.27**	**31.66**	**-13.87**	**16.15**	-1.67	1.78	-0.45	0.53
Benthodemersal elasmobranches	0.57	0.21	**-9.06**	**-8.83**	**-8.90**	-2.53	2.55	-2.11	2.19	-0.23	0.23	-0.30	0.31
Large benthodemersal fish	0.57	1.84	**-17.13**	**-16.72**	**-16.83**	**-5.86**	**6.47**	-1.83	1.83	-0.70	0.75	-0.31	0.33
Seabirds	0.00	4.61	**-35.80**	**-34.98**	**-35.22**	**7.68**	**-7.99**	4.28	-4.33	-3.31	3.50	0.57	-0.71
Dolphins and other marine mammals	0.03	0.35	**-9.03**	**-8.90**	**-8.95**	-2.64	2.71	-0.30	0.30	-0.84	0.88	0.42	-0.46

Discussion and conclusions

Among the scenarios examined, three of the nutrient load ones (MFA, RBE, REB) showed the largest changes compared to BAU, however among them the changes were almost irrelevant. The simulated changes in the nutrient inputs had in general a negative effect on the system, as seen by the reduction in several metrics and in biomasses. The level of change compared to BAU was substantial for these three scenarios, especially given the short time span examined here.

The time series of the different metrics under the fisheries related scenarios followed similar patterns with BAU but positively or negatively shifted, depending on the change in fishing effort/mortality. Still, the level of change seemed generally low. The biomasses of the FGs also showed lower responses to the stresses caused by fisheries (at least the ones examined here) than in the nutrient load scenarios. In general the system showed lower changes under the fisheries scenarios compared to the nutrient driven ones. Our results show that the system is more resilient to changes in fisheries than to changes affecting the LTL organisms. These changes are not reflected on the biomasses of LTL but are transferred up the food-web affecting the biomasses of HTL. It should be further explored whether the higher response to the nutrient load scenarios is related to the fact that flows among LTL groups dominate the system and the model's (and metrics) response is more sensitive to nutrient changes than to modifications on the fisheries, or whether the level of stress is simply lower in the specific fisheries scenarios examined here.

The metrics that reflected changes under the nutrient scenarios were related to all ecosystem attributes (except exploitation) but there was not a common pattern for all; FiB index increased while Catch, Kempton's W, FCI and SfG decreased. In contrast, as concerns fisheries scenarios the metrics affected the most were the ones related to catches and/or exploitation and seemed to change as a direct effect of modifications in fishing effort/mortality. Moreover, there was not the same level of sensitivity for all metrics and some didn't reveal changes in the system. These highlights the importance of using a set of indicators instead of just one when assessing ecosystem status or attributes (in our case resilience), as already proposed by several authors (e.g., Christensen, 1995; Coll *et al.*, 2016) and the indicators should be also chosen in relation to the type of stress/change.

References

Christensen, V. 1995. Ecosystem maturity -- towards quantification. Ecological Modelling, 77(1), 3-32.

Christensen, V., Walters, C. J. 2004. Ecopath with Ecosim: methods, capabilities and limitations. Ecological Modelling, 172, 109–139.

Coll M., L. J. Shannon, K. M. Kleisner, M. J. Juan-Jordá, A. Bundy, A. G. Akoglu, D. Banaru, J. L. Boldt, M. F. Borges, A. Cook, I. Diallo, C. Fu, C. Fox, D. Gascuel, L. J. Gurney, T. Hattab, J. J. Heymans, D. Jouffre, B. R. Knight, S. Kucukavsar, S. I. Large, C. Lynam, A. Machias, K. N. Marshall, H. Masski, H. Ojaveer, C. Piroddi, J. Tam, D. Thiao, M. Thiaw, M. A. Torres, M. Travers-Trolet, K. Tsagarakis, I. Tuck, G. I. van der Meeren, D. Yemane, S. G. Zador and Y. J. Shin, 2016. Ecological indicators to capture the effects of fishing on biodiversity and conservation status of marine ecosystems. Ecological Indicators, 60, 947-962.

Costanza, R., Mageau, M., 1999. What is a healthy ecosystem? Aquatic Ecology, 33: 105–115.

EU 2008. Directive 2008/56/EC of the European Parliament and of the council. Establishing a framework for community action in the field of marine environmental policy (Marine Strategy Framework Directive). Official Journal of the European Union.

Heymans, J. J., Coll, M., Libralato, S., Morissette, L., Christensen, V. 2014. Global Patterns in Ecological Indicators of Marine Food Webs: A Modelling Approach. PLoS ONE, 9(4), e95845.

Lazzari, P., Solidoro, C., Ibello, V., Salon, S., Teruzzi, A., Béranger, K., Crise, A., 2012. Seasonal and inter-annual variability of plankton chlorophyll and primary production in the Mediterranean Sea: a modelling approach. Biogeosciences, 9(1): 217-233

Libralato, S., Coll, M., Tudela, S., Palomera, I., Pranovi, F. 2008. Novel index for quantification of ecosystem effects of fishing as removal of secondary production. Marine Ecology Progress Series, 355, 107-129.

Libralato, S., Solidoro, C., 2009. Bridging biogeochemical and food web models for an End-to-End representation of marine ecosystem dynamics: The Venice lagoon case study. Ecological Modelling, 220(21): 2960-2971.

Lynam, C. P., Mackinson, S. 2015. How will fisheries management measures contribute towards the attainment of Good Environmental Status for the North Sea ecosystem? Global Ecology and Conservation, 4, 160-175.

Tsagarakis K, Coll M, Giannoulaki M, Somarakis S, Papaconstantinou C, Machias A. 2010. Food-web traits of the North Aegean Sea ecosystem (Eastern Mediterranean) and comparison with other Mediterranean ecosystems. Estuarine, Coastal and Shelf Science 88: 233-248.

Black Sea

NW-Black sea LTL coastal modelling (ULg-MARE)

The resilience assessment for this region of the Black Sea is reported in deliverables D4.8 (Food web analysis at the regional and basin scale) and D4.12 (Report on SES environmental status based on modelling and remote sensing tools).

NW-Black sea LTL coastal modelling (focus on Varna region) (USOF)

The resilience assessment for this region of the Black sea is reported in deliverable D4.12 (Report on SES environmental status based on modelling and remote sensing tools).

Basin scale HTL Modelling -(METU)

The resilience assessment for the Black Sea at the basin scale is reported in deliverables D4.8 (Food web analysis at the regional and basin scale) and D4.12 (Report on SES environmental status based on modelling and remote sensing tools).

PERSEUS
POLICY-ORIENTED MARINE
ENVIRONMENTAL RESEARCH IN
THE SOUTHERN EUROPEAN SEAS